









Apocarotenoids are allosteric effectors of a dimeric plant glycosyltransferase involved in defense and lignin formation

Guangxin Sun^{1*}, Jieren Liao^{1*}, Elisabeth Kurze¹ , Timothy D. Hoffmann¹ , Wieland Steinchen² ,
Kate McGraphery¹ , Ruth Habegger¹ , Ludwig Marek¹, Dragana A. M. Catici³, Christina Ludwig⁴ ,
Tingting Jing⁵, Thomas Hoffmann¹, Chuankui Song⁵ , and Wilfried Schwab¹ 

¹Biotechnology of Natural Products, School of Life Sciences Weihenstephan, Technische Universität München, Liesel-Beckmann-Str. 1, 85354 Freising, Germany; ²Center for Synthetic Microbiology (SYNMIKRO) & Faculty of Chemistry, Philipps-University Marburg, Karl-von-Frisch-Straße 14, 35043 Marburg, Germany; ³Center for Protein Assemblies (CPA), Technical University of Munich, Ernst-Otto-Fischer-Str. 8, 85748 Garching, Germany; ⁴Bavarian Center for Biomolecular Mass Spectrometry (BayBioMS), School of Life Sciences Weihenstephan, Technische Universität München, Gregor-Mendel-Str. 4, 85354 Freising, Germany; ⁵State Key Laboratory of Tea Plant Biology and Utilization, International Joint Laboratory on Tea Chemistry and Health Effects, Anhui Agricultural University, 230036 Hefei, Anhui, China

Summary

Authors for correspondence:
Wilfried Schwab
Email: wilfried.schwab@tum.de

Chuankui Song
Email: sckfriend@163.com

Received: 18 October 2022
Accepted: 2 March 2023

New Phytologist (2023) 238: 2080–2098
doi: 10.1111/nph.18875

Key words: apocarotenoids, effector, glycosyltransferase, ionol, lignin, phytoalexin.

- Glycosyltransferases are nature's versatile tools to tailor the functionalities of proteins, carbohydrates, lipids, and small molecules by transferring sugars. Prominent substrates are hydroxycoumarins such as scopoletin, which serve as natural plant protection agents. Similarly, C13-apocarotenoids, which are oxidative degradation products of carotenoids/xanthophylls, protect plants by repelling pests and attracting pest predators.
- We show that C13-apocarotenoids interact with the plant glycosyltransferase NbUG-T72AY1 and induce conformational changes in the enzyme catalytic center ultimately reducing its inherent UDP- α -D-glucose glucohydrolase activity and increasing its catalytic activity for productive hydroxycoumarin substrates. By contrast, C13-apocarotenoids show no effect on the catalytic activity toward monolignol lignin precursors, which are competitive substrates.
- *In vivo* studies in tobacco plants (*Nicotiana benthamiana*) confirmed increased glycosylation activity upon apocarotenoid supplementation. Thus, hydroxycoumarins and apocarotenoids represent specialized damage-associated molecular patterns, as they each provide precise information about the plant compartments damaged by pathogen attack.
- The molecular basis for the C13-apocarotenoid-mediated interplay of two plant protective mechanisms and their function as allosteric enhancers opens up potential applications of the natural products in agriculture and pharmaceutical industry.

Introduction

Apocarotenoids are molecules that constitute the specialized (or secondary) metabolism of organisms. They are produced by carotenoid cleavage dioxygenases (CCDs) and nonenzymatic processes from carotenoid and xanthophyll (oxy-functionalized carotenoids) precursors, which are formed in photosynthetic organisms (Hou *et al.*, 2016). The central role of carotenoids in plants and humans has led to significant efforts to understand their metabolism (Nisar *et al.*, 2015). While the carotenoid biosynthesis pathway has been well studied, the enzymatic degradation of carotenoids and xanthophylls could only be proven by identification of viviparous14 (VP14) in 1997 and has been intensively investigated since then (Schwartz *et al.*, 1997). Viviparous14 is the first CCD enzyme found to catalyze the

formation of an apocarotenoid by regiospecific cleavage of xanthophylls. In recent decades, more and more apocarotenoids and their functions have been discovered (Hou *et al.*, 2016). Among them are the plant hormones abscisic acid (ABA) and strigolactones, the vitamin A derivatives retinal and retinol, the pigments norbixin, bixin, crocetin and crocin, the bitter tastant picrocrocin, and volatiles such as β -ionone and β -damascenone, which contribute to the aroma of rose scent. The C10 apocarotenoid safranal is isolated from the spice saffron, and other C13 apocarotenoids (norisoprenoids) are found in leaves of numerous plants (Beltran & Stange, 2016). They serve as chemoattractants, repellents, growth stimulators, growth inhibitors, promote intra-, and interspecies interactions, and regulate plant architecture and growth. Tobacco plants (*Nicotiana* spp.) are a particularly rich source of apocarotenoids such as C13 derivatives, since α -ionol/ionone, β -ionol/ionone, and α -/ β -damascenone have been isolated from their essential oils (Enzell, 1985).

*These authors contributed equally to this work.

Apocarotenoids carrying hydroxyl or carboxyl functional groups are subject to further modifications including methylation and glycosylation catalyzed by methyltransferases and glycosyltransferases, respectively.

Similarly, hydroxycoumarins including scopoletin (7-hydroxy-6-methoxycoumarin) and umbelliferone (7-hydroxy-6-coumarin) are secondary metabolites produced by many plant species including *Nicotiana* ssp. (Stringlis *et al.*, 2019). They function as iron-mobilizing substances, show antimicrobial and antiviral activities, and play an important role in pathogen defense as phytoalexins (Chong *et al.*, 2002). Hydroxycoumarins also act as semiochemicals in aboveground and belowground plant-microbe interactions, and in compositions of the root microbiome. After their production, coumarins are found as free aglycone or in modified form by hydroxylation, methylation, and glycosylation (Stringlis *et al.*, 2019).

Glycosylation is mediated by enzymes that transfer sugars from activated donor saccharides to acceptor molecules including small molecules (Bowles *et al.*, 2006). The sugar donors are most frequently activated nucleotide carbohydrates, such as uridine 5'-diphosphate α -D-glucopyranose (UDP-glucose). Glycosylation of small molecules derived from the specialized metabolism alters their physicochemical properties, for example, water solubility, stability, volatility, transport characteristics, and thus bioactivity and bioavailability. Large multigene families encode plant enzymes involved in the sugar transfer to small molecules. They show a conserved signature motif in their primary sequence known as plant secondary (specialized) product glycosyltransferase (PSPG) box, which groups them among family 1 glycosyltransferases (GT1; <http://www.cazy.org/GlycosylTransferases.html>). GT1, also known as UDP glycosyltransferases (UGTs), is the most important GT family in the plant kingdom (Yonekura-Sakakibara & Hanada, 2011). One UGT can often transform more than one substrate but several UGT enzymes can glycosylate the same acceptor (Bowles *et al.*, 2006).

The 3D structures of glycosyltransferase published to date adopt the GT-A, GT-B, GT-C, or GT-D folds (Zhang *et al.*, 2014), while plant UGTs show a GT-B fold and transfer sugars by an inverting glycosylation mechanism (Liang *et al.*, 2015). GT-B fold members bind the acceptor and carbohydrate donor in the N- and C-terminal domains, respectively, and the protein undergoes a number of conformational changes during the reaction. The structural changes alter the size and shape of the active site and generate the actual binding sites (Liang *et al.*, 2015). A histidine residue at the beginning of the N-terminal domain serves as a catalytic base for the deprotonation of the hydroxyl group on the acceptor molecule. This enables a nucleophilic attack at the anomeric center of the sugar donor (Offen *et al.*, 2006).

UGTs play a central role in plant development and growth, as they are involved in various specialized metabolic pathways. UGTs are implicated in the homeostasis of plant hormones such as abscisic acid and auxins, regulate plant pathogen defense through glycosylation of phytoalexins, and play a role in the biosynthesis of lignin, although their exact function in lignin formation is not yet clear. Before the formation of lignin, the monolignols coumaryl, coniferyl, and sinapyl alcohols/aldehydes must be translocated into the cell wall, but they are glucosidically

bound in the cytosol (Wang *et al.*, 2013; Le Roy *et al.*, 2016). Two glycosyltransferases from *Arabidopsis thaliana* UGT72E2 and UGT72E3 glucosylate monolignols at the 4-O position (Lanot *et al.*, 2006). Downregulation of *UGT72E2* and *UGT72E3* reduced monolignol glucoside concentrations in transgenic *Arabidopsis* plants, and *UGT72E1* and *UGT72E2* are co-expressed with the cell wall-resident peroxidases *PRX49* and *PRX72* (Le Roy *et al.*, 2016). The results indicate that glycosyltransferases are essential for plant cell wall lignification.

During a study of the monolignol/phytoalexin NbUGT72AY1 (Sun *et al.*, 2019, 2020; Liao *et al.*, 2022), we detected substrate inhibition by the acceptor-substrate scopoletin at 4 μ M and discovered the enzyme's promiscuous activity for C13-apocarotenoids. Detailed investigations revealed significant UDP-glucose glucosehydrolase activity of the protein, which was inhibited by apocarotenoids. By contrast, the addition of apocarotenoids increased the enzymatic activity of NbUGT72AY1 toward productive hydroxycoumarins. Detailed biochemical analyses combined with hydrogen/deuterium exchange mass spectrometry (HDX-MS) revealed contrasting conformational changes at the N-terminal H1 helix of the protein carrying the catalytically active His in the presence of the acceptor and effector molecules. The HDX results confirmed that the binding of apocarotenoids and hydroxycoumarins to the protein triggered different structural changes near the catalytic site, thereby altering the catalytic activity. Finally, application of apocarotenoids to tobacco seedlings increased the production of scopoletin- β -D-glucoside, confirming the biological consequences of the newly discovered molecular mechanism.

Materials and Methods

Chemicals

All chemicals were purchased from Sigma-Aldrich, Merck (Darmstadt, Germany), Carl Roth (Karlsruhe, Germany), and Thermo Fisher Scientific (Dreieich, Germany) unless otherwise noted. Uridine 5'-diphosphate glucose (UDP-glucose) was obtained from Sigma-Aldrich. All substrates used for enzymatic reactions, including those employed for substrate screening via liquid chromatography-mass spectrometry (LC-MS), UDP-Glo™ Glycosyltransferase Assay, and Glucose-Glo™ Assay (both Promega), were diluted in dimethyl sulfoxide (DMSO).

Heterologous expression and purification of UGT72AY1

Total RNA was isolated from *Nicotiana benthamiana* leaves. The gene coding for *NbUGT72AY1* (NbV6.1trP2283, <http://bentgenome.qut.edu.au/>) was amplified from cDNA (Sun *et al.*, 2019). Isolation of *NbUGT73A24* and *NbUGT73A25* was performed as described by Sun *et al.* (2019). For the His-tagged variant, the corresponding PCR fragment of *NbUGT72AY1* was ligated via *NheI/XhoI* sites into the pET28b vector. For recombinant protein production, *Escherichia coli* BL21(DE3)pLysS cells were used (Sun *et al.*, 2020). The fusion protein with the N-terminal GST-tag was purified using GST Bind resin (Merck).

After cell disruption by sonification, the crude protein extract was incubated for 3 h at 4°C with the resin. The recombinant NbUGT72AY1 was eluted with GST elution buffer (50 mM Tris–HCl pH 8.0; 10 mM reduced glutathione). The fusion protein with the N-terminal His-tag was purified using Profinity™ IMAC Ni-Charged Resin (Bio-Rad). The recombinant His-tagged NbUGT72AY1 was eluted with His elution buffer (50 mM sodium phosphate buffer pH 7.4, 300 mM NaCl, 500 mM Imidazol) and then buffer exchanged to the GST elution buffer (50 mM Tris–HCl pH 8.0) using PD-10 column (Cytiva, Freiburg im Breisgau, Germany). The protein concentration was determined in microtiter plates (Rotilabo® F-Profil; Carl Roth) using Roti®-Nanoquant following the manufacturer's instructions (Carl Roth) with bovine serum albumin (BSA) as standard protein. Absorption at 450 and 590 nm was detected with the CLARIOstar plate reader (BMG Labtech, Ortenberg, Germany). The purity of the recombinant protein was verified by SDS-PAGE. Oligomeric states of the recombinant proteins were verified by NATIVE-PAGE.

Qualitative and quantitative substrate screening via LC–MS and UDP-Glo™ glycosyltransferase assay

The UGT reaction assay for the qualitative screening by LC–MS consisted of 50 µl crude protein extract, 600 µM substrate, and 1 mM UDP-glucose in a total volume of 200 µl 100 mM Tris–HCl buffer (pH 7.5). The reaction was initiated by the addition of the sugar donor and incubated with constant shaking at 400 rpm, in the dark at 30°C for 17 h. The reaction was stopped by heating 10 min at 75°C and centrifuged twice at 25 000 g for 10 min. Enzymatically formed products were analyzed by LC–MS according to Sun *et al.* (2019). Based on the results of the qualitative substrate screening, positive substrates were selected and quantitatively tested using the UDP-Glo™ Glycosyltransferase Assay (Promega). One microgram of purified NbUGT72AY1 was incubated with 100 µM substrate in 50 mM Tris–HCl (pH 7.5) in a final volume of 100 µl. The reaction was started by adding 100 µM UDP-glucose and incubated at 30°C for 20 min. To quantify the free UDP released during the reaction catalyzed by UGT, equal volumes of the UGT reaction assay and UDP detection reagent (UDR) were mixed in a 384-well plate (384 Well Plates Corning 4513; Sigma-Aldrich) and incubated in the dark at room temperature for 60 min. Luminescence was measured using the CLARIOstar plate reader. For the blank reaction, 1 µl DMSO was added instead of substrate solution. The values of this no-(acceptor) substrate control were subtracted from the substrate readings as a background luminescence signal.

General procedure for determination of UDP- α -glucose glucohydrolase and glycosyltransferase activity of NbUGT72AY1 and inhibition and enhancement of activities by effectors

The assay consisted of 0.4–5 µg purified NbUGT72AY1 (NbUGT73A24 or NbUGT73A25), 0–200 µM scopoletin (acceptor substrate), 0–1200 µM α -ionol, β -ionol, α -ionone, or

β -ionone (effectors) in 50 mM Tris–HCl (pH 7.5) in a final volume of 100 µl. The reaction was started by adding 0–100 µM UDP-glucose (donor substrate) and incubated at 30°C for 20 min. After incubation, 12.5 µl inactivation solution was directly added to the reactions (100 µl) to stop the reaction and the solution was centrifuged at 50 g for 5 min according to McGraphery & Schwab (2020). Next, 12.5 µl neutralization solution was added, centrifuged at 50 g for 1 min, and stored at –20°C. Before analysis of the solutions using UDP-Glo™ Glycosyltransferase Assay and Glucose-Glo™ (Promega), all samples were thawed at room temperature and centrifuged at 20 000 g for 15 s. Then, 5 µl of the UGT reactions was added to 5 µl UDR and 5 µl glucose detection reagent (GDR), respectively, mixed by gently shaking for 30–60 s, and incubated in the dark at room temperature for 60 min. Luminescence was measured with CLARIOstar plate reader and UDP and glucose concentrations were calculated according to the manufacturer's instructions. Triplicates were performed for each measurement.

Hydrogen deuterium exchange mass spectrometry (HDX-MS)

HDX-MS was conducted essentially as described previously (Liao *et al.*, 2022). Ligands were employed as 50 mM concentrated stock solutions dissolved in DMSO (α -ionol, α -ionone, β -ionol, β -ionone, and scopoletin). In a first experiment probing the effect of individual ligands on NbUGT72AY1, purified GST-NbUGT72AY1 was mixed with 1% (v/v) ligand stock solutions to achieve final concentrations of 35 µM GST-NbUGT72AY1 and 500 µM ligand, respectively, and incubated for 5 min at ambient temperature. In a second experiment probing the combined effects of scopoletin and apocarotenoids, purified GST-NbUGT72AY1 was mixed with 1% (v/v) per ligand stock solution or DMSO to achieve final concentrations of 35 µM GST-NbUGT72AY1 and 500 µM for each ligand, respectively, and incubated for 5 min at ambient temperature. The final DMSO concentration in this experiment was thus 2% (v/v).

Preparation of HDX reactions for was aided by a two-arm robotic autosampler (LEAP Technologies, Carrboro, NC, USA). Protein solution in the respective ligand-bound state (7.5 µl) was mixed with 67.5 µl of D₂O-containing buffer, which contained 20 mM Tris–Cl pH 7.5 supplemented with the respective ligands at 500 µM final concentration, resulting in 1% or 2% (v/v) final DMSO concentration in experiment 1 and 2, respectively. This mixture was incubated for 10/30/95/1000/10 000 s at 25°C, after which the HDX reaction was quenched by addition of an equal volume of 400 mM KH₂PO₄/H₃PO₄ supplemented with 2 M guanidine-HCl (pH of 2.2) at 1°C. Ninety-five microliter of the resulting mixture was injected into an Acquity UPLC M-class system with HDX technology (Waters, Milford, MA, USA). GST-NbUGT72AY1 was digested online with a column containing porcine pepsin and separated by reversed-phase HPLC followed by mass spectrometric analysis as described previously (Liao *et al.*, 2022). Peptides were identified with the PROTEIN-LYNX GLOBAL SERVER (Waters) software as described previously. For quantification of deuterium incorporation with DYNAMX

v.3.0 (Waters), peptides had to fulfill the following criteria: minimum intensity of 10 000 counts; minimum number of products of three; maximum mass error of 25 ppm; and retention time tolerance of 0.5 min. After automated data processing by DYNAMX 3.0, the mass spectra were manually inspected and, if necessary, peptides omitted, for example, in case of low signal-to-noise ratio or presence of overlapping peptides. HDX-MS raw data are supplied as a source file (Supporting Information Dataset S1) as recommended by Masson *et al.* (2019).

In planta experiments

Nicotiana benthamiana seeds were grown on sterile Murashige–Skoog (MS) culture in sterile glasses covered with sterile caps (Murashige & Skoog, 1962). Thirty milliliter of the culture medium were treated with 200 μM scopoletin in combination with various additives (α -ionol, β -ionol, α -ionone, and β -ionone, each 200 μM). All substances were diluted with DMSO and filter-sterilized. Dimethyl sulfoxide (control), 200 μM scopoletin, and the additives alone were added to the medium. Five seeds per glass were placed with a sterile tweezer on the surface of the medium with equal distance to each other to assure optimal plant growth. Each treatment was repeated five times (total 25 seedlings per treatment). After 7 wk, growth of the tobacco plants was documented. An average day and night temperature of 25°C and 22°C, respectively, was set with alternating light cycles of 12 h and 12 h dark cycles. The average lighting intensity was 1.46 klux. All glasses were placed on the shelf in a random order of seven rows and 16 columns calculated with the random generator of MS Excel to compensate uneven lighting conditions. Plant features such as the height and fresh weight were evaluated. Tobacco plants were harvested, frozen in liquid nitrogen, and stored at -80°C for further analysis. Lyophilized plant material was used for extraction. After addition of 2 ml methanol, containing 25 $\text{ng } \mu\text{l}^{-1}$ 4-methylumbelliferyl- β -D-glucuronide as an internal standard, vortexing, and sonication for 10 min, the sample was centrifuged at 16 000 g for 10 min. The supernatant was removed, and the residue was re-extracted 2 \times with 2 ml methanol each. The supernatants were combined, concentrated to dryness in a vacuum concentrator, and re-dissolved in 50 μl 80% methanol. After vortexing, sonication for 10 min, and centrifugation at 16 000 g for 10 min, the clear supernatant was used for LC–MS analysis.

LC–MS analysis

An Agilent 6340 Ion Trap mass spectrometer (Agilent Technologies, Santa Clara, CA, USA) connected to an Agilent 1200 HPLC system equipped with a capillary pump and a diode array detector was utilized. Components were separated with a Phenomenex Luna C18(2) column (150 mm long \times 2.0 mm i.d., particle size 5 μm , 100 \AA ; Phenomenex, Aschaffenburg, Germany) that was held at 28°C. LC was performed with the following binary gradient system: solvent A, water with 0.1% formic acid and solvent B, and 100% methanol with 0.1% formic acid. The gradient program was as follows: 0–30 min, 100% A to

50% A/50% B; 30–35 min, 50% A/50% B to 100% B, hold for 15 min; 100% B to 100% A, in 5 min, and then hold for 10 min. Injection volume was 5 μl , and the flow rate was 0.2 ml min^{-1} . The ionization parameters were as follows: the voltage of the capillary was 3500 V and the end plate was set to -500 V. The capillary exit was 121 V, and the Octopole RF amplitude 171 Vpp. The temperature of the dry gas (N_2) was 330°C at a flow of 9 l min^{-1} and the nebulizer pressure 30 psi. Tandem MS was carried out using helium as the collision gas (4×10^{-6} mbar) with 1 V collision voltage. Scan range was from m/z 50 to 975 with a scan resolution of 26 000 m/z . Spectra were acquired in positive and negative ionization mode, and target ions were fragmented in auto MS2 mode. Metabolites were identified by their retention times, mass spectra, and product ion spectra in comparison with the data determined for authentic reference materials. Relative metabolite quantification was performed using the DATAANALYSIS v.4.0 (Build 234) and QUANTAANALYSIS v.2.0 (Build 234) software (Bruker Daltonik GmbH, Bremen, Germany). The results were normalized to the internal standard.

LC–MS/MS-based analysis of recombinant protein gel bands

Recombinant generated NbUGT72AY1-GST and NbUGT72AY1-His were run on native and SDS-based protein gels. Protein bands were excised out of the gel, reduced (50 mM DTT), alkylated (55 mM chloroacetamid), and digested overnight with trypsin (trypsin-gold; Promega). The generated peptides were dried in a vacuum concentrator and dissolved in 25 μl 0.1% formic acid (FA). LC–MS/MS measurements were performed on an Ultimate 3000 RSLCnano system coupled to a Q-Exactive HF-X mass spectrometer (Thermo Fisher Scientific). For each analysis, 3 μl of peptides were delivered to a trap column (ReproSil-pur C18-AQ, 5 μm , Dr Maisch, 20 mm \times 75 μm , self-packed) at a flow rate of 5 $\mu\text{l min}^{-1}$ in 100% solvent A (0.1% formic acid in HPLC grade water). After 10 min of loading, peptides were transferred to an analytical column (ReproSil Gold C18-AQ, 3 μm , Dr Maisch, 400 mm \times 75 μm , self-packed) and separated using a 50 min gradient from 4% to 32% of solvent B (0.1% formic acid in acetonitrile and 5% (v/v) DMSO) at 300 nl min^{-1} flow rate. Both nanoLC solvents contained 5% (v/v) DMSO. The Q-Exactive HF-X mass spectrometer was operated in data-dependent acquisition and positive ionization mode. MS1 spectra (360–1300 m/z) were recorded at a resolution of 60 000 using an automatic gain control (AGC) target value of $3e^6$ and maximum injection time (maxIT) of 45 ms. After peptide fragmentation using higher energy collision-induced dissociation (HCD), MS2 spectra of up to 18 precursor peptides were acquired at a resolution of 15 000 with an AGC target value of $1e^5$ and maxIT of 25 ms. The precursor isolation window width was set to 1.3 m/z and normalized collision energy to 26%. Dynamic exclusion was enabled with 25 s exclusion time (mass tolerance \pm 10 ppm). Peptide identification and quantification were performed using MAXQUANT (v.1.6.3.4). MS2 spectra were searched against an *E. coli* BL21 (DE3) protein database

plus the protein sequence from the overexpressed target protein NbUGT72AY1, as well as the amino acid sequences of the two fused tags (His-tag and GST-tag). Furthermore, the protein database was supplemented with common contaminants (built-in option in MAXQUANT). Carbamidomethylated cysteine was set as fixed modification and oxidation of methionine and N-terminal protein acetylation as variable modifications. Trypsin/P was specified as proteolytic enzyme. Precursor tolerance was set to 4.5 ppm and fragment ion tolerance to 20 ppm. Results were adjusted to 1% false discovery rate on peptide spectrum match and protein level employing a target-decoy approach using reversed protein sequences. The minimal peptide length was defined as seven amino acids; the 'match-between-run' function was not enabled. Estimations of protein mass fractions were carried out using the 'intensity-based absolute quantification' function implemented in MAXQUANT.

Sedimentation velocity analytical ultracentrifugation

Sedimentation velocity analytical ultracentrifugation (SV-AUC) experiments were performed on a Beckman Coulter Optima™ AUC analytical ultracentrifuge (Beckman Coulter, Brea, CA, USA) equipped with absorbance optics. For each sample, 350 µl of 2 µM Fc4-GST and Fc4-His in 50 mM Tris-HCl buffer, pH 8 were loaded into a standard 12 mm double-sector epon-filled centerpiece, respectively, covered with quartz windows, alongside with 450 µl of the reference buffer solution. Samples were centrifuged at 840 000 *g* using an An-50 Ti rotor at 20°C (with an initial test run at 60 000 *g*). Radial absorbance scans were acquired continuously at 280 nm with a radial step size of 0.001 cm. The obtained sedimentation velocity profiles were analyzed using SEDFIT software with a nonmodel-based continuous Svedberg distribution method (*c*(*s*)) (Dam *et al.*, 2005). The density (ρ) and viscosity (η) of the Tris-HCl buffer used for data analysis were experimentally determined using an Anton Paar Density Meter DMA 5000 M and an Anton Paar Automated Micro Viscometer, respectively.

Protein modeling

Homology modeling of NbUGT72AY1 was performed using the ALPHAFOLD (Jumper *et al.*, 2021) tool implemented in CHIMERA X (v.1.4, <https://www.cgl.ucsf.edu/chimerax/>). Ligand docking (UDP-glucose and scopoletin) was performed by AUTODOCK VINA (<http://vina.scripps.edu/>) using CHIMERA (v.1.16, <https://www.cgl.ucsf.edu/chimera/>) for visualization. Default values were used.

Data analysis

The Michaelis–Menten equation (Eqn 1) was employed to calculate K_m and v_{max} values for UDP- α -D-glucose glucosyltransferase activity of NbUGT72AY1 using KALEIDAGRAPH (v.4.5.4; Synergy, Reading, PA, USA).

$$v = \frac{v_{max} \times \frac{[S]}{K_m}}{1 + \frac{[S]}{K_m}} \quad \text{Eqn 1}$$

Here, v is the rate of product formation, v_{max} is maximal velocity, $[S]$ is substrate concentration, and K_m is the Michaelis constant. The goodness of fit of all numerical values was assessed using the correlation coefficient R , the standard error values of the parameters (parameter value \pm error), and the chi-squared values (sum of squared errors between the original data and the calculated curve fit). The kinetic constants are reported as the value \pm standard error of the parameter estimate. To calculate the kinetics in the case of ionol/ionone-induced inhibition of the UDP-glucose glucosyltransferase activity and induced amplification of the glucosyltransferase activity, a modified equation (Eqn 2) was used in which v_0 is the initial reaction velocity and k_1 is equal the effector concentration at $v_{max}/2$.

$$v = \frac{v_0 + v_{max} \times \frac{[S]}{K_1}}{1 + \frac{[S]}{K_1}} \quad \text{Eqn 2}$$

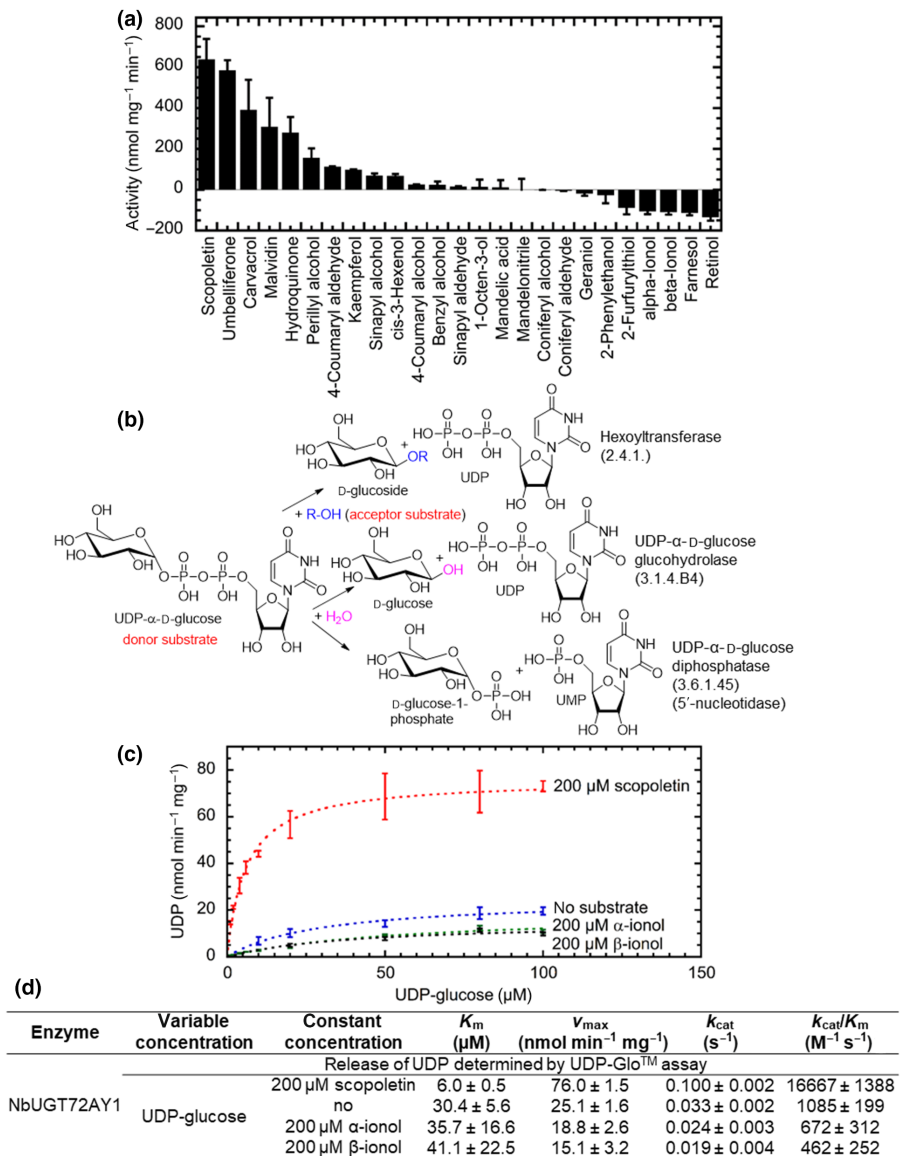
Results

NbUGT72AY1 shows a considerable UDP- α -D-glucose glucosyltransferase activity

In a recent study characterizing the substrate specificities of UGTs from *N. benthamiana*, NbUGT72AY1 was identified as a promiscuous enzyme capable of glucosylating a wide range of small molecules, including phenolics (monolignols and hydroxycoumarins), isoprenoids (monoterpenoids and apocarotenoids), and aliphatic alcohols (hexanols and octanols), as shown by LC–MS analysis (Sun *et al.*, 2019; Figs S1–S3). Since the LC–MS data did not allow straightforward comparison of the catalytic activity of NbUGT72AY1 toward different substrates due to the varying ionizability of the products, we used the UDP-Glo™ assay, which quantifies the release of UDP during glucoside formation and thus allows a direct comparison of the enzymatic activity (Fig. 1a,b). The release of UDP is first quantified in mixtures containing the enzyme and the donor and acceptor substrates (Fig. 1b). The amount of UDP in the control consisting of only the enzyme and the donor substrate (no-acceptor control) is then subtracted from this value.

The UDP-Glo™ assay confirmed the results of the LC–MS-based substrate screening but delivered negative values for three apocarotenoids (α -ionol, β -ionol, and retinol), a sesquiterpenoid (farnesol), and a thiol (2-furfurylthiol), probably due to the subtraction of a very high background signal for the control (no-acceptor substrate) sample. Since the production of α -ionol and β -ionol β -D-glucosides by NbUGT72AY1 has already been confirmed by LC–MS analysis (Sun *et al.*, 2019; Fig. S1), we concluded that a high UDP-forming activity, in the absence of acceptor, could explain the contrasting results of the LC–MS and UDP-Glo™ analyses. Furthermore, farnesol, retinol, and

Fig. 1 NbUGT72AY1 shows uridine 5'-diphosphate α -D-glucopyranose (UDP-glucose) glucohydrolase and glycosyltransferase activity. Substrate screening of NbUGT72AY1 using the uridine 5'-diphosphate glucose (UDP-GloTM) assay (a). Reaction catalyzed by Hexosyltransferase, UDP- α -D-glucose glucohydrolase, and UDP- α -D-glucose diphosphatase (b). Michaelis–Menten kinetics of NbUGT72AY1 using increasing concentration of UDP-glucose and constant (200 μ M) concentration of scopoletin, α -, and β -ionol or no substrate (c). Eqn 1 was used for the calculation. Kinetic data of UDP production by NbUGT72AY1 from UDP-glucose at constant (200 μ M) concentration of scopoletin, α -, and β -ionol or no substrate (d). Scopoletin is glucosylated and α -, and β -ionol reduce the inherent UDP- α -D-glucose glucohydrolase activity of NbUGT72AY1, whereby the formation of the corresponding β -D-glucosides can also be detected by liquid chromatography–mass spectrometry (LC–MS). Error bars represent \pm SD.



2-furfurylthiol did not act as substrates but showed negative values. UDP- α -D-glucose glucohydrolase activity has been demonstrated for a number of glycosyltransferases (Fig. 1b; Cieśla & Bobak, 1998; Rangarajan *et al.*, 2009; Sheikh *et al.*, 2017; Levanova *et al.*, 2019) in addition to UDP-glucose diphosphatase (5'-nucleotidase) activity (Carter *et al.*, 2018). UDP-glucose titration alone and in the presence of 200 μ M scopoletin proved the UDP-forming, UDP- α -D-glucose glucohydrolase activity of NbUGT72AY1 (k_{cat}/K_m 1085 $\text{M}^{-1} \text{s}^{-1}$), and its scopoletin glycosyltransferase activity (k_{cat}/K_m 16 667 $\text{M}^{-1} \text{s}^{-1}$), respectively.

However, reduced UDP-forming activity (k_{cat}/K_m 672 $\text{M}^{-1} \text{s}^{-1}$ and 462 $\text{M}^{-1} \text{s}^{-1}$ for α - and β -ionol, respectively) was determined in the presence of α -ionol and β -ionol (Fig. 1c,d). It should be noted that at 200 μ M scopoletin, NbUGT72AY1 is clearly inhibited by the acceptor substrate (Liao *et al.*, 2022).

The formation of UDP and glucose by NbUGT72AY1 from UDP-glucose in the absence of acceptor substrates, representing

UDP- α -glucose glucohydrolase activity, was further confirmed by concurrent UDP-GloTM and Glucose-GloTM assays, respectively (Fig. S4A). NbUGT72AY1 has considerable UDP-glucose glucohydrolase activity compared with two related enzymes (NbUGT73A24 and NbUGT73A25) that also hydrolyze UDP-glucose but to a minor extent (Fig. S4B). The kinetic parameters determined by the UDP-GloTM and Glucose-GloTM assays were not statistically different. Therefore, in the absence of an alcohol acceptor molecule, water can act as an alternative acceptor, releasing identical molar amounts of UDP and glucose.

The UDP- α -glucose glucohydrolase activity of NbUGT72AY1 is partially noncompetitively inhibited by apocarotenoids

To clarify the inhibition mechanism of the ionols on the glucohydrolase activity of NbUGT72AY1, UDP-glucose titration in the

presence of different ionol concentrations (20 and 200 μM) was performed and the release of UDP and glucose determined (Fig. S4C). Michaelis–Menten saturation curves were obtained (Eqn 1). Noncompetitive inhibition (K_m^{app} unchanged; v_m^{app} decreased) was derived from kinetic data calculated from the quantities of released UDP and glucose (Fig. S4D). Ionols are competitive inhibitors of the substrate water but inhibit uncompetitive when the concentration of the second substrate (UDP-glucose) is varied in case of an ordered sequential two-substrate reaction (Luukkainen *et al.*, 2005). Noncompetitive inhibition by ionols as shown by the Glo™ assays clearly indicates that ionols bind to the free enzyme and the enzyme/substrate (NbUGT72AY1/UDP-glucose) complex with similar affinity. The release of UDP and glucose was reduced more by β -ionol than by α -ionol.

Slopes and intercepts of the Lineweaver–Burk plots derived from the UDP-glucose glucohydrolase inhibition data were calculated to distinguish between partial and complete inhibition (Fig. S5A). Since the slope and intercept replots for β -ionol are curved, a partial noncompetitive inhibition can be assumed (Fig. S5B; Grant, 2018). In the case of α -ionol, the conclusion is not as clear. The kinetics calculated from the Lineweaver–Burk plots (Fig. S5C) are consistent with the values in Fig. S4(D).

Titration experiments were performed with ionols and their corresponding ionones in the presence of a constant concentration of UDP-glucose to test the inhibitory effect of α - and β -ionone, both of which are nonproductive substrates of NbUGT72AY1, on the UDP-glucose glucohydrolase activity (Fig. S6A, B). An equation assuming that binding of the effectors reduces the enzyme activity in a manner similar to the Michaelis–Menten equation fits the curves best (Eqn 2). When measuring the UDP release, the ionones showed higher K_I^{eff} values (97.2 and 33.2 μM for α - and β -ionone, respectively) than the corresponding ionols (32.6 and 26.5 μM for α - and β -ionol, respectively). However, their $v_{\text{max}}^{\text{eff}}$ values (4.5 and 5.0 $\text{nmol min}^{-1} \text{mg}^{-1}$ vs 6.6 and 5.5 $\text{nmol min}^{-1} \text{mg}^{-1}$, respectively) were alike. Similar data were obtained with the Glucose-Glo™ assay measuring the release of glucose. The results confirm that apocarotenoids inhibit UDP-glucose glucohydrolase activity in a concentration-dependent manner, with α -ionone having the lowest affinity and activity-diminishing potency.

Apocarotenoids enhance the glucosyltransferase activity of UGT72AY1 to hydroxycoumarins but not to monoglignols

We next analyzed the effect of different concentrations of apocarotenoid effectors on the glucosyltransferase activity of NbUGT72AY1 towards the preferred substrate scopoletin (Fig. 2a). The apocarotenoids increased the catalytic activity of the UGT toward this hydroxycoumarin in a concentration-dependent manner (upper part of Fig. 2a) although the glucohydrolase activity was inhibited in the absence of scopoletin (lower part of Fig. 2a). The Michaelis–Menten kinetic parameters were calculated for the curves using Eqn 2 (Fig. 2b,c). For example, the apparent maximum velocity of NbUGT72AY1 ($v_{\text{max}}^{\text{app}}$) rose from 21 to 67.9 $\text{nmol min}^{-1} \text{mg}^{-1}$ with increasing addition of β -ionol,

whereas the β -ionol concentration at which the reaction rate was 50% of $v_{\text{max}}^{\text{app}}$ was calculated to be 49.9 μM (K_I^{eff}). We conclude that the enzyme substrate complexes with allosterically bound apocarotenoids form and release scopoletin glucoside more rapidly than the enzyme substrate complex without effector ligands. This effect is stronger for the ionols than for ionones (Fig. 2a).

The effect of co-incubation of α - and β -ionol on scopoletin and ionol glucoside formation was analyzed by LC–MS (Fig. S7). NbUGT72AY1 catalyzed the formation of the corresponding glucosides when scopoletin or the ionol substrates and UDP-glucose were available. Co-incubation of scopoletin in the presence of the ionols resulted in enhanced formation of scopoletin glucoside (Fig. S7), whereas formation of the ionol glucosides was suppressed (Fig. S7). In the presence of UDP, glucoside formation was reduced in each case by product inhibition, whereas glucose did not affect glucoside catalysis.

Further LC–MS analyses independently confirmed enhanced formation of scopoletin glucoside by NbUGT72AY1 in the presence of apocarotenoids (α - and β -ionol, α - and β -ionone, and α - and β -damascone; Fig. S8). While in the control experiment the peak area of scopoletin glucoside accounted to 6.5% of the substrate scopoletin, the addition of 100 μM β -ionol increased the product yield to 44.5%. Similarly, carotenoid degradation products promoted the production of umbelliferone glucoside by NbUGT72AY1 (Fig. S9). However, the formation of coniferyl aldehyde glucoside was not affected by C13-apocarotenoids (Fig. S10).

The unexpected activation of the catalytic activity of NbUGT72AY1 toward hydroxycoumarin derivatives by plant secondary metabolites was further studied as function of UDP-glucose concentration (Fig. 3a). With increasing UDP-glucose and β -ionol concentrations, enhanced release of UDP and thus elevated formation of hydroxycoumarin glucosides was observed. The Lineweaver–Burk plot shows parallel lines, but the replot of slopes and axis intercepts does not exhibit straight lines (Fig. 3b–d). Both $v_{\text{max}}^{\text{app}}$ and K_m^{app} increased with increasing β -ionol concentration (0–200 μM) from 67.8 to 110.8 $\text{nmol min}^{-1} \text{mg}^{-1}$ and from 17.7 to 28.4 μM , respectively (Fig. 3e). Similarly, after addition of 200 μM α -ionol and β -ionone, elevated glycosylation activity of NbUGT72AY1 was observed for scopoletin, with an increase in K_m^{app} , whereas the effect of α -ionone was less pronounced. This indicates partial uncompetitive activation of NbUGT72AY1 by the apocarotenoids.

NbUGT72AY1 forms different types of stable multimers depending on the protein tag but this does not affect the kinetics of the enzyme

To exclude the possibility that the GST-tag is involved in the activation of NbUGT72AY1 by ionols, we also produced the His-tagged UGT. Determination of the oligomeric state of His-tagged NbUGT72AY1 by native-PAGE and analytical ultracentrifugation revealed a monomeric and a dimeric form of 62.5 and 110 kDa, respectively (Fig. S11A). On native gels, the size of the proteins can only be roughly estimated, but

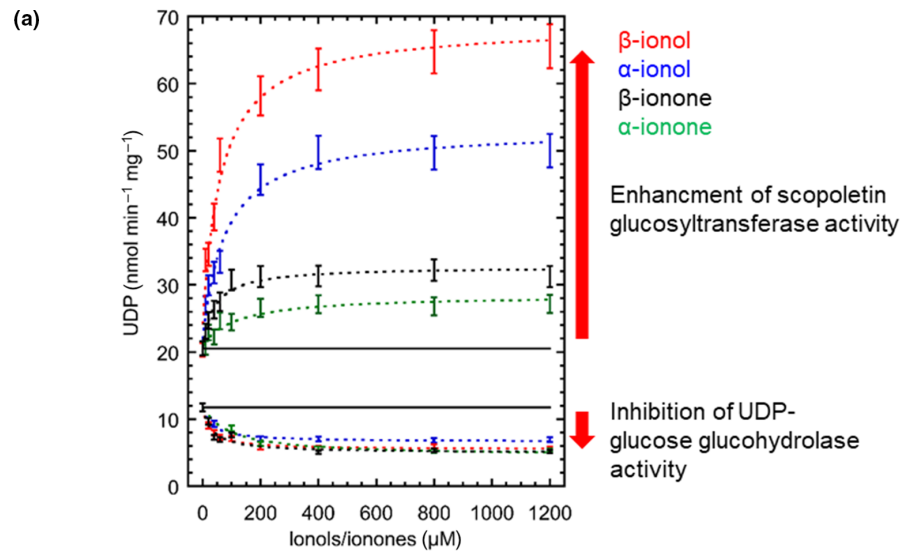


Fig. 2 Enhancement of the uridine 5'-diphosphate α -D-glucopyranose (UDP-glucose):scopoletin glucosyltransferase activity of NbUGT72AY1 by ionols and ionones as a function of ionol/ionone concentration. Inhibition of the UDP-glucose glucosyltransferase activity and amplification of the glucosyltransferase activity of NbUGT72AY1 are concentration dependent (a). Release of UDP was determined using the uridine 5'-diphosphate glucose (UDP-GloTM) assay. Kinetic data were obtained by fitting to Eqn 2. KALEIDAGRAPH 4.5.4 was used for fitting the data. Inhibition of the UDP-glucose glucosyltransferase activity (b) and amplification of the glucosyltransferase activity of NbUGT72AY1 (c). Error bars represent \pm SD.

(b) Inhibition of UDP-glucose glucosyltransferase activity

Enzyme	Variable concentration	Constant concentration	v_{max}^{app} (nmol min ⁻¹ mg ⁻¹)	K_I^{app} (μ M)	R
Release of UDP determined by UDP-Glo TM assay					
NbUGT72AY1	α -ionol	100 μ M UDP-glucose	6.6 \pm 0.1	32.6 \pm 4.5	0.99
	α -ionone		4.5 \pm 0.4	97.2 \pm 26.5	0.99
	β -ionol		5.5 \pm 0.1	26.5 \pm 3.2	0.99
	β -ionone		5.0 \pm 0.4	33.2 \pm 8.7	0.97

(c) Enhancement of UDP-glucose:scopoletin glucosyltransferase activity

Enzyme	Variable concentration	Constant concentration	v_{max}^{app} (nmol min ⁻¹ mg ⁻¹)	K_I^{app} (μ M)	R
Release of UDP determined by UDP-Glo TM assay					
NbUGT72AY1	α -ionol	100 μ M UDP-glucose	53.6 \pm 1.3	99.4 \pm 16.2	0.99
	α -ionone		27.7 \pm 0.5	66.1 \pm 17.4	0.97
	β -ionol	200 μ M scopoletin	67.9 \pm 1.7	49.9 \pm 8.1	0.99
	β -ionone		32.5 \pm 0.4	35.3 \pm 5.5	0.99

based on the MS-identified proteins in the gel bands, the formation of a monomeric and dimeric form is assumed. The affinity-purified GST-tagged protein showed at least four bands on the native-PAGE gel and three bands after thrombin digestion. Five proteins were separated by analytical ultracentrifugation for purified GST-tagged UGT (Fig. S11B). Assignment of the bands was achieved by LC-MS/MS (Fig. S12). LC-MS/MS-identified peptides derived mainly from GST and NbUGT72AY1 in bands 3, 4, and 5. Most likely, those bands represent the trimer (221 kDa), dimer (142 kDa), and monomer (73.8 kDa) form of the fusion protein NbUGT72AY1-GST. The theoretical sizes do not agree well with the marker sizes in this case either, for the reason already mentioned. Band 6 of 49.7 kDa (Fig. S11B) probably contains dimeric GST, untagged NbUGT72AY1, HSP70 of *E. coli*, and other proteins (Fig. S12). Although the protein tags resulted in distinct oligomeric states of the NbUGT72AY1 protein, the differentially tagged proteins did not differ in their UDP-glucose glucosyltransferase and UGT activities (Fig. S13).

Hydrogen/deuterium exchange mass spectrometry (HDX) discloses that apocarotenoids and scopoletin trigger opposite conformational changes in NbUGT72AY1

Before HDX-MS of NbUGT72AY1 was performed, the 3D structure of the protein was predicted by ALPHAFOLD (Jumper *et al.*, 2021; Fig. 4a). The majority of structural features of NbUGT72AY1 were predicted with high confidence (predicted local distance difference test, pLDDT > 90), whereas helix 2, and loops between strand β 9 and α 14, β 8, and α 13, β 10 and 16 α , and β 7 and α 12 showed pLDDT < 90 (Fig. 4a). The latter appear to be the most flexible segments of the protein skeleton and seal off the catalytic center. Scopoletin docking was performed on the predicted 3D model of NbUGT72AY1 using the Autodock Vina tool implemented in UCSF Chimera and the donor analog UDP-2F-glucose was added by matching the predicted structure with 2vce (rcsb.org; Fig. 4a).

To elaborate on substrate and effector binding to NbUGT72AY1 in solution, we performed hydrogen/deuterium exchange

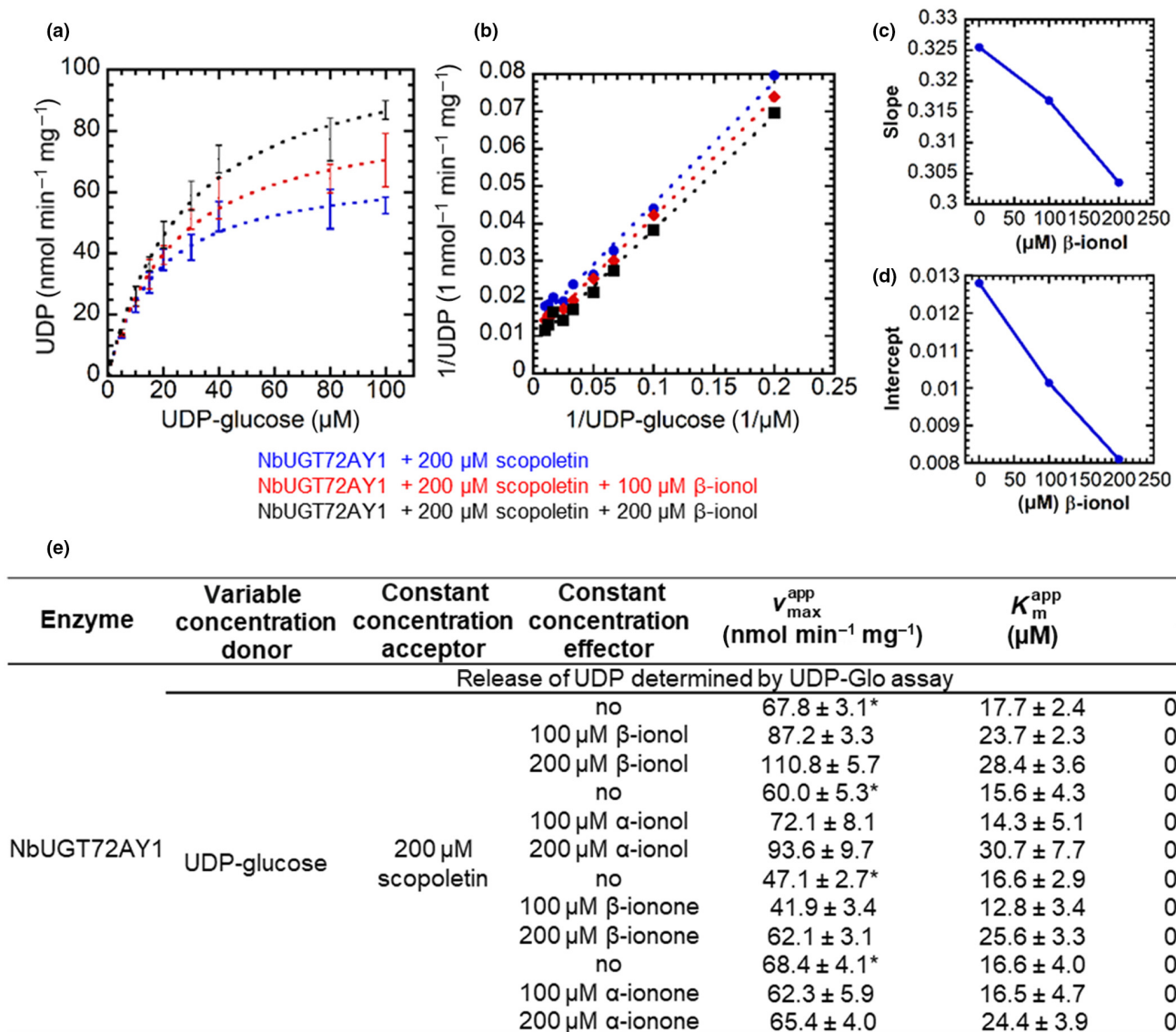


Fig. 3 Activation of the uridine 5'-diphosphate α-D-glucopyranose (UDP-glucose):scopoletin glucosyltransferase activity of NbUGT72AY1 by acarotenoids as a function of UDP-glucose concentration. Activation of the glucosyltransferase activity of NbUGT72AY1 by β-ionol is concentration dependent (a). Lineweaver-Burk plot (b) and slopes (c) and intercepts (d) of the straight lines. Release of UDP was determined using the uridine 5'-diphosphate glucose (UDP-Glo™) assay. Kinetic data were obtained by fitting to Eqn 1 (e). KALEIDAGRAPH 4.5.4 was used for fitting. *, Data for the no-effector controls of the individual experiments. Error bars represent ± SD.

mass spectrometry (HDX-MS) in solution. HDX-MS provides insights into protein structure, conformational changes upon ligand or protein binding, and function (Masson *et al.*, 2019). HDX-MS determines mass shifts due to isotopic exchange between amide hydrogens of the protein backbone and solvent D₂O. The rate of isotope substitution depends on the folded state and the dynamics of the protein (the stability of hydrogen bridge networks), and the physicochemical characteristics of the corresponding amino acid sequence (Koner mann *et al.*, 2011).

In HDX-MS experiments, proteins dissolved in buffer are diluted in similarly buffered D₂O solvents, resulting in labile hydrogens of the protein being exchanged with deuterium of the D₂O. The exchange rate depends not only on pH and temperature, but also on protein structure and dynamics because

hydrogen atoms may be protected from exchange with solvent deuterium atoms due to tertiary structure or hydrogen bonding.

The rate of exchange is measured by acquiring MS data at multiple intervals after exposure to D₂O, resulting in profiles of deuterium uptake vs time that reflect conformation and dynamics under specific conditions, such as the presence or absence of a ligand. Deuterium uptake is often recorded after quenching of the exchange reaction, followed by proteolytic digestion before LC/MS-based analysis. The advantage of this approach is that it imparts a degree of 'spatial resolution' to the data, usually in segments averaging about five amino acid residues.

The effects of scopoletin and UDP binding on the structure of NbUGT72AY1 were previously analyzed by HDX-MS (Liao *et al.*, 2022). In the present study, NbUGT72AY1 was subjected

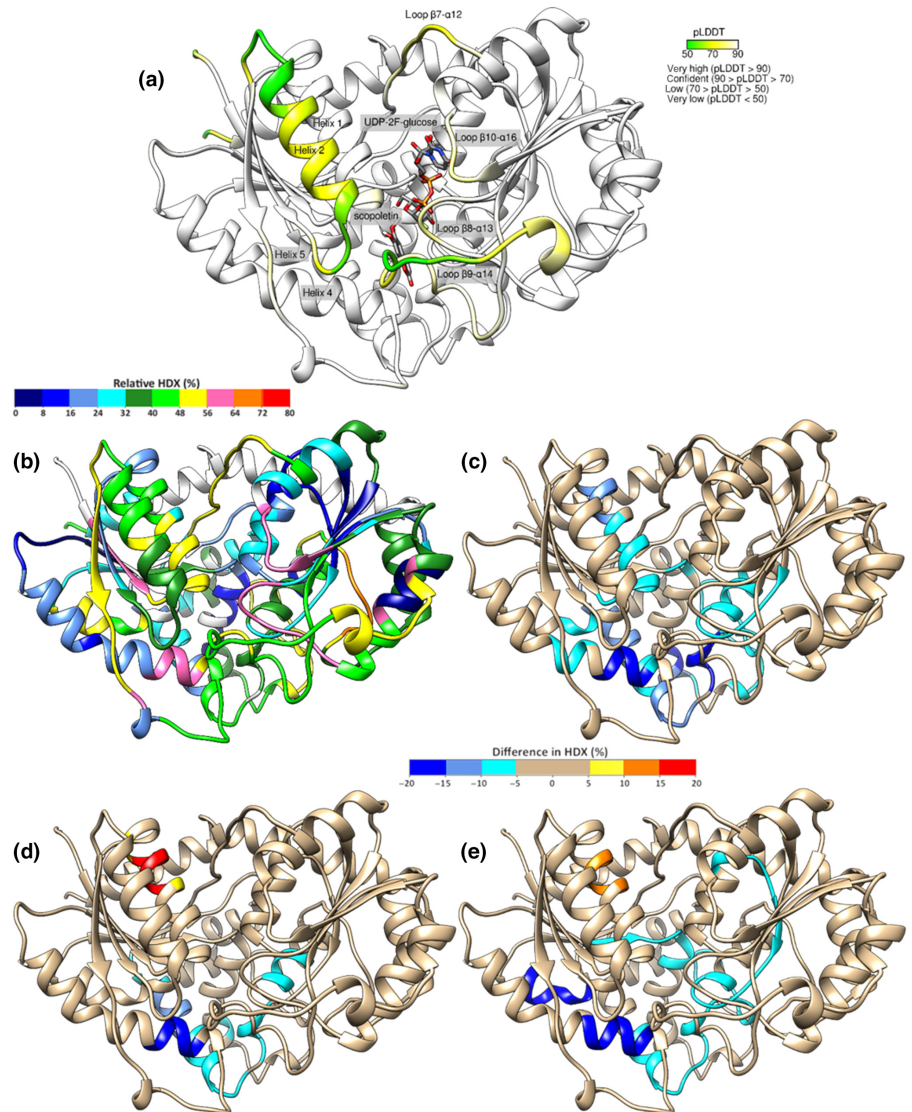


Fig. 4 NbUGT72AY1 3D structure predicted by AlphaFold. The predicted local distance difference test (pLDDT) result on a scale from 0 to 100 is mapped onto the predicted 3D structure (a). Color-coded relative deuterium uptake of apo NbUGT72AY1 after 10 000 s (b). Differential hydrogen/deuterium exchange (HDX) results obtained after the addition of scopoletin (c), β -ionol (d), and combination of both (e) to the protein are color-mapped onto the predicted 3D structure of NbUGT72AY1.

to HDX-MS in the absence and in presence of scopoletin and/or effector ligands. Approximately 240 peptides were detected after deuterium labeling of the protein and pepsin digestion, covering *c.* 91% of the GST-tagged NbUGT72AY1 protein (Dataset S1). The pattern of deuterium incorporation by GST-NbUGT72AY1 showed low deuteration in the N-terminal GST portion of the fusion protein but high deuterium exchange in the loop connecting GST to NbUGT72AY1. For the NbUGT72AY1 portion, 50% HDX were apparent already after 10 s of deuteration for areas predicted to be unstructured, for example, aa 245–255, 277–284, 305–328, and 409–414, whereas areas with predicted secondary structures incorporated deuterium less readily (Figs 4b, S14). Thus, the modeled structure of NbUGT72AY1 suitably recapitulates the protein's conformation in solution and confers a reasonable dynamic range for potential differences in HDX over most regions of NbUGT72AY1.

Reduced HDX of NbUGT72AY1 in comparison with the apo state was determined upon incubation with the acceptor-substrate scopoletin in five regions of the protein (Fig. S15). These include amino acids near the catalytically active His18 in the N-terminal

domain, that is, helix 1 (aa 12–29), the N-terminal part of helix 4 (aa 87–97), the helix 5 (aa 122–125), the region from helices 6–10 (aa 154–208), and the segment from strand β 12 to helix α 18 to (aa 386–399; Fig. 4c). Most of these changes are consistent with the assumption that scopoletin is bound to the canonical acceptor site, since HDX changes are observed for His18 and near Asp118, two amino acids involved in catalysis.

The apocarotenoid ligands induced perturbations in HDX of NbUGT72AY1 in similar areas of the protein as scopoletin (e.g. for α -ionol, aa 24–30; 88–92, 165–208, and 393–397), except for helix 5 (aa 122–128; Figs S16A–S19A, 4d). The binding of α -ionone to NbUGT72AY1 is less pronounced and the effect on HDX not as prominent in the presence of this effector compared with the other ligands (Fig. S17A). However, in contrast to the changes in HDX observed for scopoletin, the interaction of all four apocarotenoids with NbUGT72AY1 promotes deuteration of aa 24–30, indicating a less rigid structure in this region in the presence of ionols/ionones (Fig. 4d). Thus, the carotenoid degradation products induce a conformational change at helix 1 that counteracts the reduced HDX caused by scopoletin. Since helix 1

carries the catalytically active His18 (Figs S15, 4), this could provide an explanation for the increased reaction rate toward scopoletin in presence of apocarotenoids (Fig. 2), although the second binding site for the apocarotenoids in addition to the active site remains indiscernible in our experiment.

Additional evidence for the importance of the identified activation site located in helix 1 is provided by a second HDX-MS experiment, in which we determined the deuterium uptake of UGT72AY1 in the presence of scopoletin and one apocarotenoid each compared with apoprotein (Figs S16B–19B, 4e). For all four possible combinations, the region of aa 24–28 showed increased HDX and thus flexibility. When calculating the differences in deuterium uptake between apocarotenoid/scopoletin-bound and scopoletin-bound NbUGT72AY1, the importance of aa 13–36 for catalysis becomes even more apparent. In the presence of ionones/ionols, the conformational mobility of this entity is greatly increased compared with apo and scopoletin-bound NbUGT72AY1 (Figs S20, S21).

Apocarotenoids reduce the inhibition of NbUGT72AY1 by the substrate scopoletin

Recently, NbUGT72AY1 was shown to exhibit non-Michaelis–Menten kinetics, which was interpreted as substrate inhibition (Liao *et al.*, 2022). To investigate the effect of apocarotenoids on the non-Michaelis–Menten kinetics of scopoletin glucosylation, we determined the formation of scopoletin glucoside in the absence and presence of apocarotenoids by LC–MS (Fig. S22). The glucosylation activity of NbUGT72AY1 toward scopoletin increased in a concentration-dependent manner when defined amounts of α -ionol/ionone and β -ionol/ionone were added (Fig. S22A). The effect of apocarotenoid alcohols was stronger than that of aldehydes. A combination of the cooperativity-describing Hill equation and the partial uncompetitive inhibition equation best described the data obtained. The addition of apocarotenoids only slightly increased the reaction rate in the inhibited state (v_i), but the inhibition constant (K_i), that is, the concentration of inhibitor required to reduce the maximum reaction rate to half of the uninhibited value, increased sharply while v_{\max} and K_m remained unaffected (Fig. S22B). Compared with the scopoletin glucosyltransferase activity of NbUGT72AY1 ($v_{\max} = 267 \pm 29 \text{ nmol min}^{-1} \text{ mg}^{-1}$), the ionol glucosylation activity is low (α -ionol $v_{\max} = 13.6 \pm 0.8 \text{ nmol min}^{-1} \text{ mg}^{-1}$ and β -ionol $v_{\max} = 5.2 \pm 0.2 \text{ nmol min}^{-1} \text{ mg}^{-1}$; Fig. S23). While β -ionol exhibits Michaelis–Menten kinetics, α -ionol shows a curve best described by complete substrate inhibition. Thus, the LC–MS data clearly demonstrate increased scopoletin glucoside production in the presence of the apocarotenoids.

Apocarotenoids increase scopoletin glucoside production by *in vitro*-grown tobacco plants after scopoletin supplementation

Finally, we tested apocarotenoid-induced enhancement of scopoletin glucosylation *in planta* using *in vitro*-grown *N. benthamiana* plants (Fig. 5a). Tobacco seeds were grown for 42 d on

Murashige–Skoog (MS) nutrient medium with each of the natural products (scopoletin, α -ionol, β -ionol, α -ionone, and β -ionone) and with combinations of scopoletin and the apocarotenoids. The solvent DMSO was used as a control. Tobacco plant phenotypic traits such as plant height, root color, and fresh weight differed compared with the control when the MS culture medium was treated with scopoletin in combination with various apocarotenoids. The addition of one plant metabolite to the medium had only a small effect on average fresh weight and shoot length, but after the addition of a second metabolite, the inhibitory effect was significant compared with the solvent control (Fig. 5b,c). Scopoletin glucoside was quantified by LC–MS in the lyophilized plants, but only the seedlings that grew in the presence of scopoletin accumulated detectable concentrations $> 0.04 \mu\text{g-eq. mg}^{-1}$ of the glucoside while it was undetectable in the control sample. Scopoletin glucoside content increased significantly in all plants supplemented with scopoletin together with apocarotenoids compared with samples containing scopoletin only, for example, to an average of $0.12 \mu\text{g eq. mg}^{-1}$ in *N. benthamiana* seedlings grown in the presence of scopoletin and β -ionol (Fig. 5d).

Discussion

NbUGT72AY1 was isolated in the course of a project addressing the substrate specificity of *N. benthamiana* UGTs using an aglycone library (Sun *et al.*, 2019). The enzyme was notable for its promiscuity, glucosylating the phytoalexin scopoletin, C13-apocarotenoids (Sun *et al.*, 2020), and monolignols (Liao *et al.*, 2022), among others.

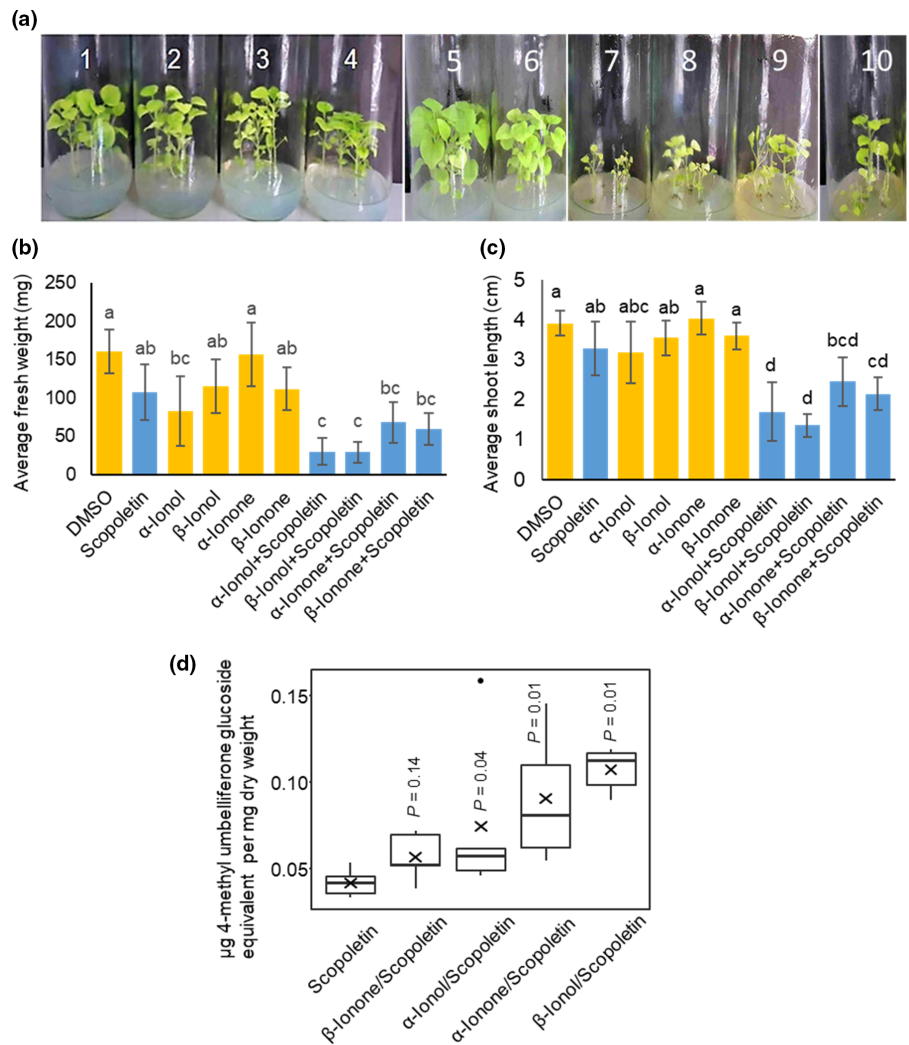
NbUGT72AY1 likely contributes to lignin biosynthesis

Members of the UGT72 family in plants generally glycosylate two classes of phenylpropanoids, (1) the monolignols, which are building blocks of lignin, the cell wall-reinforcing polyphenolic polymer, and (2) the flavonoids, which are critical in plant interactions with other organisms and responses to stress (Speeckaert *et al.*, 2022). Monolignol UGT activity was first demonstrated for UGT72 enzymes from Arabidopsis (*AtUGT72E1-3*), which have been shown to be involved in lignin biosynthesis in this model plant (Speeckaert *et al.*, 2020). An *AtUGT72E2*-knockdown mutant line (72E2KD) exhibited a twofold reduction in the amount of coniferyl alcohol 4-*O*-glucoside and sinapyl alcohol 4-*O*-glucoside compared with the wild-type and *AtUGT72E3* down-regulation affected the kinetics of lignin deposition (Lanot *et al.*, 2006; Baldacci-Cresp *et al.*, 2020). NbUGT72AY1 is also likely involved in the production of lignin, as it shares high sequence similarity with monolignol UGTs, efficiently glucosylates monolignols (Fig. S3), is mainly expressed in the stem, and its ortholog from potato is co-expressed with lignin-forming peroxidases (Liao *et al.*, 2022; Speeckaert *et al.*, 2022).

NbUGT72AY1 is probably a component of plant defense

As NbUGT72AY1 is a promiscuous enzyme and efficiently glucosylates the phytoalexin scopoletin (Fig. 1) it may also be a

Fig. 5 *In planta* experiment with *Nicotiana benthamiana*. Tobacco seeds were grown on Murashige–Skoog (MS) culture medium with various additives: dimethyl sulfoxide (DMSO) (1); scopoletin + DMSO (2), α -ionol + DMSO (3), β -ionol + DMSO (4), α -ionone + DMSO (5), β -ionone + DMSO (6), scopoletin + α -ionol (7), scopoletin + β -ionol (8), scopoletin + α -ionone (9), and scopoletin + β -ionone (10) for 42 d (a). Mean fresh weight (b) and shoot length of the seedlings (c) were determined (five seeds \times five jars and total 25 biological replicates). The orange bars in (b) and (c) indicate the control (DMSO) and apocarotenoid samples, while the blue bars show the samples with scopoletin and in combination with apocarotenoids. Error bars represent the standard deviation. The values of the bars are significantly different when none of the letters are identical (Tukey test $P < 0.05$). The relative concentration of scopoletin glucoside (in μg -equ. per mg dry weight) was quantified by liquid chromatography–mass spectrometry (LC–MS) (all seedlings of one jar were combined and extracted; four jars were used, corresponding to four biological replicates) in the seedlings (d). The P -values were calculated using the Wilcoxon test in comparison with scopoletin. Box plot graphs were constructed for the peak areas of scopoletin glucoside relative to the internal standard 4-methyl umbelliferone glucoside. A horizontal line in the boxes indicates the medians and boxes the interquartile range. Whiskers extend to 10th and 90th percentiles. Outliers are displayed by black dots.



component of *N. benthamiana* plant defense. Plants have developed numerous strategies to survive under stressful conditions. One measure is the *de novo* formation of cytotoxic phytoalexins, which are produced by the plant immediately after an attack by viruses, microorganisms, or insects (Jeandet, 2015). Similarly, biosynthesis of the coumarin derivative scopoletin, which has fungistatic, antimicrobial, and insect-repellent activity and reduces the accumulation of reactive oxygen species, is also induced following pathogen infection (Beyer *et al.*, 2019). In addition, hydroxycoumarins are essential components of the Fe acquisition system of nongrass species after secretion into the rhizosphere under low Fe bioavailability conditions (Robe *et al.*, 2021).

In tobacco, scopoletin glucoside is formed via a jasmonate- and ethylene-dependent biosynthetic pathway along with its aglycone as part of the host's rapid response to biotic and abiotic stresses (Sun *et al.*, 2017; Stringlis *et al.*, 2019). Glycosylation seems to confer an advantage to plants, because the transfer of a sugar unit protects from the cytotoxic effect of the phytoalexin and allows transport into the vacuole and translocation from the

aerial parts to the roots (Graña *et al.*, 2017). Overexpression of a scopoletin UGT73 (TOGT) in *Nicotiana tabacum* resulted in early lesion formation during the hypersensitive response to tobacco mosaic virus and had no effect on virus resistance (Gachon *et al.*, 2004). In a second study, transgenic TOGT-overexpressing tobacco plants exhibited similar formation of necrotic leaf lesions after inoculation with potato virus Y, but the levels of virus coat protein were significantly lower compared with control plants (Matros & Mock, 2004). The conflicting results are probably due to the fact that tobacco plants express multiple UGTs that glucosylate hydroxycoumarins (Sun *et al.*, 2019), and the control mechanisms of the redundant UGT activities could likely have different effects on the respective experiments.

NbUGT72AY1 shows considerable UDP-glucose glucosyltransferase activity

When determining the enzyme kinetics of NbUGT72AY1 by UDP-Glo™ glucosyltransferase assay, negative values for a

number of substrates including α - and β -ionol were obtained after subtracting the values for the no-acceptor-substrate control (Fig. 1a). However, since LC–MS studies had already shown the formation of the C13-apocarotenoid glucosides (Figs S1C,D, S7), we suspected considerable UDP-glucose glucosyltransferase activity (Fig. 1b) of the no-acceptor-substrate control. UDP-glucose titration of NbUGT72AY1 and two related UGTs coupled with quantification of released UDP and glucose confirmed the considerable nucleotide-diphosphate-sugar hydrolase activity of the enzyme compared with the two similar proteins (Fig. S4A,B). Leloir glycosyltransferases, which use activated glycosyl donors in the form of nucleotide-diphosphate-sugars, release the nucleotide product after transfer of the sugar moiety from the nucleotide sugar. If no-acceptor substrate is available, a background hydrolysis of the donor substrate often takes place in these UGTs, that is, an enzymatically catalyzed transfer of the sugar component to a water molecule (Fig. 1b; Levanova *et al.*, 2019). The magnitude of this UGT side reaction is highly variable and so far unavoidable (Sheikh *et al.*, 2017). However, the loss of precious UDP-glucose co-substrate can significantly be reduced if the acceptor substrate is added to the enzyme before the donor substrate (Fig. 1c). This could also be a biological strategy to avoid unwanted hydrolysis in the cell.

Ionol/ionone apocarotenoids inhibit the intrinsic UDP-glucose glucosyltransferase activity

The results of Fig. 1(a) suggested that the chemicals with negative values decreased the intrinsic UDP- α -glucose glucosyltransferase activity of the enzyme. UDP-glucose titration in the presence of constant ionol concentrations confirmed the inhibitory effect of apocarotenoids (Fig. 1c), which is concentration-dependent (Figs S4C, S6) but independent of the alcohol function of the compounds since the ionones also show a similar effect (Fig. S6). Detailed kinetic studies by quantitative determination of UDP and glucose release indicated partial noncompetitive inhibition of UDP-glucose hydrolase activity by the two ionols (Fig. S5). This result implies that the ionols occupy a binding site in the active site different from that of UDP-glucose and the ionols are bound even in the absence of UDP-glucose (Fig. 6). However, the ionols (Figs S4, S5) and ionones (Figs 2, S6) cannot completely inhibit the reaction rate (Fig. 6). Similarly, human blood group B galactosyltransferase hydrolyzes its donor substrate in the absence of acceptor substrate but the enzymatic hydrolysis of UDP-galactose is effectively inhibited by a substrate analog (Sindhuwinata *et al.*, 2013).

The inhibition of the side reaction of UDP-sugar-dependent glycosyltransferases could be important in the biological context of cells as it protects the co-substrate from unwanted degradation. In animals, in addition to its function as sugar donor, UDP-glucose is well-established as a signaling molecule (van Janse Rensburg & van den Ende, 2017). In plants, preliminary studies suggest similar functions, such that UDP-glucose homeostasis is of paramount importance and inhibitors of the intrinsic UDP-glucose glucosyltransferase activity of UGTs may be important metabolic tools.

C13-apocarotenoids enhance UDP-glucose:(hydroxyl) coumarin glucosyltransferase activity of NbUGT72AY1 *in vitro* and *in planta*

After demonstrating that ionols/ionones are noncompetitive inhibitors of the intrinsic UDP-glucose glucosyltransferase activity of NbUGT72AY1, we discovered that apocarotenoids could significantly increase the hydroxycoumarin glucosyltransferase activity of the tobacco enzyme (Fig. 2). At 200 μ M acceptor and 100 μ M donor substrate, α -ionone, β -ionone, α -ionol, and β -ionol increased the maximum reaction rate (v_{\max}) from 20.5 $\text{nmol min}^{-1} \text{mg}^{-1}$ (without effector) to 27.7, 32.5, 53.6, and 67.9 $\text{nmol min}^{-1} \text{mg}^{-1}$, respectively. Detailed examination of the kinetic data revealed partial noncompetitive activation of glucosyltransferase activity (Figs 3, 6; Grant, 2018). Thus, we conclude that apocarotenoids bind not only in the active site of the enzyme, as shown by the formation of ionol glucosides (Figs S1C,D, S7), but also at an allosteric site distant from the catalytic center (Fig. 6b). This result and the findings from the kinetic data on ionol/ionone-dependent inhibition of UDP-glucose glucosyltransferase activity can be combined in a general model (Fig. 6a).

Small effector molecules (modulators, including inhibitors, and activators) that alter the activity of catalytic proteins after noncovalent binding to allosteric sites have been known almost as long as the enzymes themselves (Monod *et al.*, 1965; Cornish-Bowden, 2014).

Naturally occurring allosteric sites that regulate the catalytic activity of enzymes in primary metabolism by binding of feedback effectors have been studied in detail (Hardy & Wells, 2004), and drug discovery studies have revealed new allosteric binding sites (Bruder *et al.*, 2020) for which no natural ligands are yet known (Zorn & Wells, 2010). In addition, numerous studies have shown that the activities of P450 enzymes and glycosyltransferases in humans are regulated by ligands that bind to allosteric sites, with inhibitors being by far the largest group (Grancharov, 2001; Uchaipichat *et al.*, 2008; Fischer & Smieško, 2021). By contrast, allosteric modulators of plant secondary metabolism enzymes have not been widely studied. In *Fragaria vesca*, binding of calcium/calmodulin to an anthocyanidin UGT was shown to promote anthocyanin accumulation by reducing substrate inhibition (Peng *et al.*, 2016). Because substrate inhibition of NbUGT72AY1 was recently described for scopoletin, apocarotenoids might enhance glycosyltransferase activity of the enzyme by inhibiting scopoletin substrate inhibition in a manner similar to calmodulin (Liao *et al.*, 2022).

Although plant secondary metabolites can act as effective regulators of plant growth and defense, their molecular mechanism has not been elucidated, with the exception of phytohormones, which bind to proteins and initiate a signaling cascade after conformational change in the receptors (Erb & Kliebenstein, 2020). Volatile secondary metabolites such as terpenoids, green leaf volatiles, and aromatic compounds are released upon biotic and abiotic stress and directly induce and activate hormonal defense signaling pathways and resistance (Salt *et al.*, 1986; Wyatt, 1992; Bouwmeester *et al.*, 2019; Murata *et al.*, 2019). The precise role of secondary metabolites at physiological concentrations has not

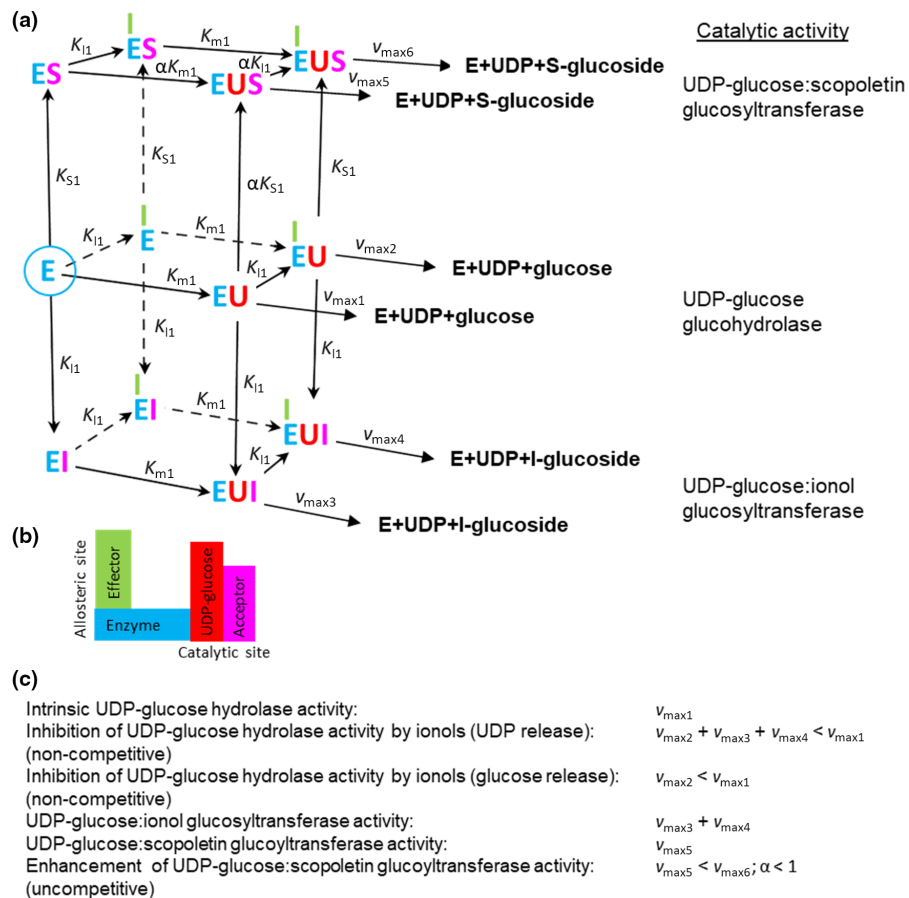


Fig. 6 Scheme presenting the uridine 5'-diphosphate α -D-glucopyranose (UDP-glucose) glucosyltransferase, UDP-glucose:scopoletin glucosyltransferase activity of NbUGT72AY1. Reactions catalyzed by NbUGT72AY1 (a). Enzyme with allosteric and catalytic binding site as shown in A (b). Conclusions derived from the results of the experiments (c). E, enzyme (+H₂O); U, UDP-glucose (donor); I, ionol (effector and acceptor); S, scopoletin (acceptor). Dashed lines are to illustrate the 3D structure.

yet been explored in detail, but their biological activity has been demonstrated clearly through chemical complementation. Our results prove that secondary metabolites such as C13-apocarotenoids bind enzymes that play an important role in plant defense mechanisms and increase the production of defense-related metabolites in the plant (Fig. 5d) while inhibiting undesirable side reactions. (Fig. 2).

Ionol/ionone apocarotenoids affect the flexibility and dynamics of helix 1 involved in acceptor-substrate binding

HDX-MS detects changes in protein conformation and 3D structural dynamics that have occurred in response to protein functions such as ligand binding and catalysis. Thus, HDX-MS helps to locate regions within an enzyme where changes in flexibility may play a key role in catalysis (Masson *et al.*, 2019). Few UGTs have been examined by HDX-MS (Zhang *et al.*, 2022). HDX-MS of NbUGT72AY1 showed relative deuterium uptake of > 56% within 10 000 s in five regions (aa 8–12, 87–92, 277–283, 347–353, and 428–433; Fig. S14) corresponding to amino acids near the N-terminus, in the acceptor binding site, of the interdomain linker, at the beginning of the PSPG box, and after the PSPG box, respectively (Fig. 4). Other highly flexible regions in the apoprotein include segment parts β 1- α 1, α 3- β 3, α 7- α 8, β 7- α 12, α 14- α 15, as well as helix 2 that seal the active site after the transition from open to closed conformer (Harrus *et al.*,

2018). Binding of scopoletin reduced HDX of helices 1, 4, and 5 adjacent to the acceptor binding site, but also of amino acids distant from the active site (aa 154–208), indicating that these regions undergo conformational change after substrate binding (Fig. 4c). The effector β -ionol seems to occupy a similar binding site to scopoletin, as similar amino acids are altered in their deuterium exchange compared with the apoenzyme, except helix 5 (Fig. 4d). However, the most revealing change occurs within helix 1, which carries the catalytically active His 18. Whereas helix 1 adopts a rigid structure after scopoletin binding, this secondary structure appears to remain more flexible in the presence of β -ionol (and the other apocarotenoids tested). This conformational mobility is not disrupted by the simultaneous presence of scopoletin (Fig. 6e). Similarly, benzyl alcohol increased deuterium uptake of regions within α -helices of a therapeutic protein (Zhang *et al.*, 2015). Although the result did not clearly identify the allosteric binding site, HDX-MS revealed amino acids that are critical for enzyme dynamics and catalysis. We hypothesize that the dynamic of helix 1 is causally related to the observed enhancement of glucosyltransferase activity.

Possible biological significance of enhanced enzymatic glucosyltransferase activity

Hydroxycoumarins and ionols/ionones are plant secondary products that have been shown to be involved, among others, in

plant protection against pathogens (Beyer *et al.*, 2019; Murata *et al.*, 2019; Brambilla *et al.*, 2022). While scopoletin is formed *de novo* by ortho-hydroxylation of feruloyl CoA after expression of a 2-oxoglutarate-dependent dioxygenase (Kai *et al.*, 2008) in response to biotic and abiotic stress, ^{13}C -apocarotenoids are produced by CCDs after digestion of carotenoid/xanthophyll-rich cell compartments (Huang *et al.*, 2009; Paparella *et al.*, 2021). Overexpression of a phytoene synthase gene resulted in overproduction of β -carotene in *Arabidopsis* roots, which was enzymatically and nonenzymatically cleaved to apocarotenoid aldehydes that were subsequently reduced to alcohols or saturated aldehydes and oxidized to acids (Koschmieder *et al.*, 2021). In addition to its aglycone, scopoletin glucoside was produced in host plants after fungal infection in even higher amounts than scopoletin. Since scopoletin glucoside has only slightly weaker antifungal activity than scopoletin, it is also considered an important factor in pathogen defense (Sun *et al.*, 2014) and studies with

scopoletin-UGT-depleted plants confirmed that glucosyltransferase activity is important for disease resistance (Stringlis *et al.*, 2019). After induction of its biosynthesis, scopoletin is synthesized in the aerial part of the plant and then translocated to the root (Gutiérrez-Mellado *et al.*, 1996). Furthermore, scopoletin glucoside concentration increased significantly in phloem sap of phytoplasma-infected mulberry plants (Gai *et al.*, 2014). Thus, coumarin derivatives are distributed in the plant after infection, contributing to systemic acquired resistance and induced systemic resistance (Kim *et al.*, 2000; Romera *et al.*, 2019).

Apocarotenoids are abundant secondary metabolites in tobacco plants (Wahlberg & Enzell, 1987) implicated in plant defense (Salt *et al.*, 1986). Similarly to the hydroxycoumarins, they accumulate after biotic stress (Wyatt, 1992). Carotenoids are relatively stable in their natural microenvironment, where they occur protein-bound or in crystalline form, but are very sensitive to oxidation or isomerization by light when the tissue is

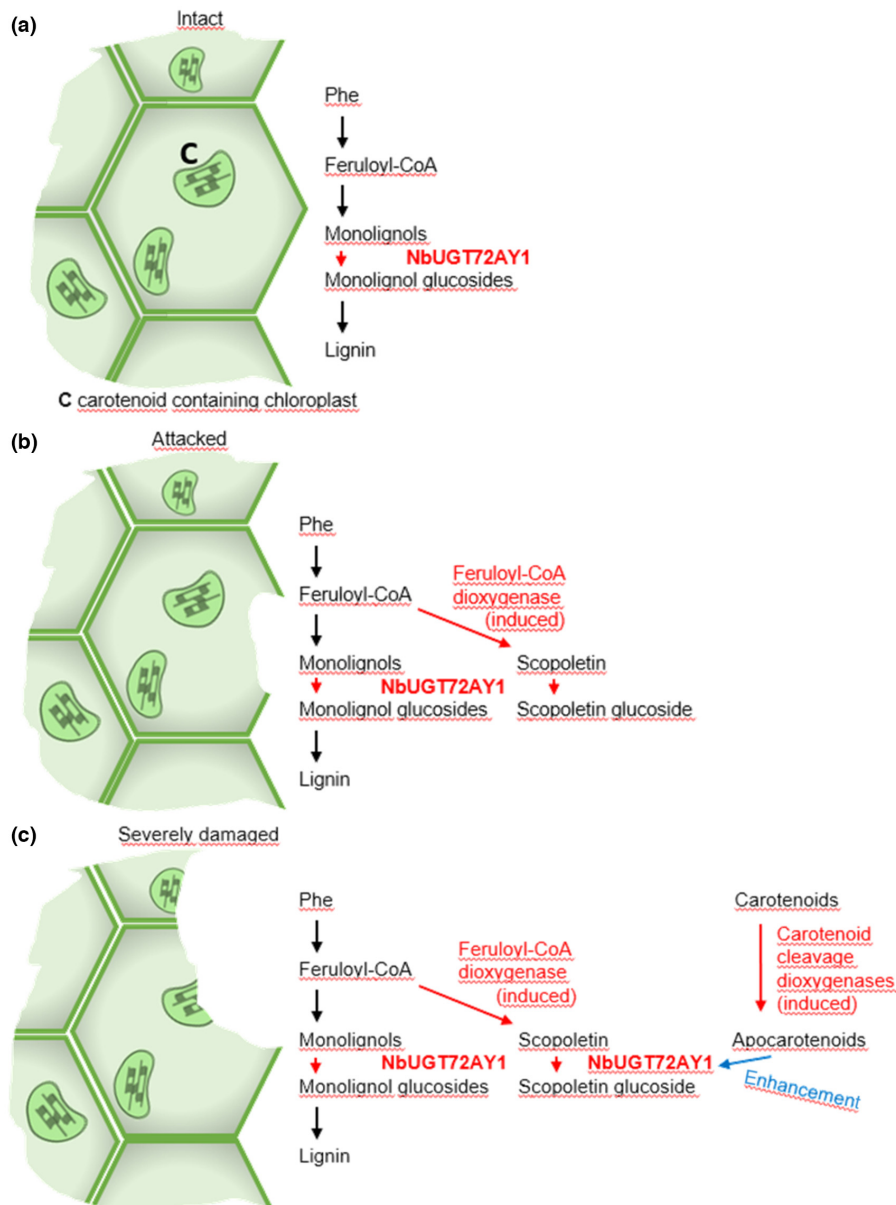


Fig. 7 Predicted role of NbUGT72AY1 in plant defense. A scheme showing three different scenarios of plant cells. In intact cells, NbUGT72AY1 contributes to the formation of lignin due to its monolignol glucosyltransferase activity (a). In cells of mildly damaged tissue, in which most chloroplasts are still intact, NbUGT72AY1 also glucosylates scopoletin (b). In severely damaged cell, scopoletin uridine 5'-diphosphate (UDP) glycosyltransferases (UGT) activity is enhanced by binding to apocarotenoids, which are carotenoid-derived metabolites produced by degradation of plastids (c).

disrupted (Torres-Montilla & Rodriguez-Concepcion, 2021). Plastids are the organelles for carotenoid biosynthesis and storage in plant cells, which also protect them from oxidative degradation by reactive oxygen species. Damage to tissues, cells, and plastids exposes carotenoids to oxygen, resulting in nonenzymatic and enzymatic degradation to apocarotenals, including ionones and ionols (Hou *et al.*, 2016; Sun *et al.*, 2018).

The production of scopoletin glucoside by tobacco plants after supplementation of the medium with hydroxycoumarin proves that the aglycone is taken up by the plant, converted to the glucoside, and accumulated, since scopoletin glucoside was not detectable in plants that were not supplemented (Fig. 5d). Addition of apocarotenoids significantly increased scopoletin glucoside concentration in treated seedlings (Fig. 5d). This result supports the hypothesis that apocarotenoids can enhance the glycosylation activity of NbUGT72AY1 *in vivo* but cannot yet provide definitive evidence, as alternative explanations are conceivable. Although most of the volatile ionones and ionols are probably lost through evaporation and metabolism during the 42 d experimental period, effects on plant growth were observed (Fig. 5b,c). This was particularly evident with the simultaneous administration of scopoletin. The elevated scopoletin glucoside levels after concomitant administration of the apocarotenoids indicate that sufficient scopoletin was present in the medium over the 42 d experimental period and that the glucoside is not subject to high turnover but rather accumulates.

All previous studies have independently examined the effects of both secondary metabolite classes on plant performance after infection, although hydroxycoumarins and apocarotenoids are produced side by side in tobacco plants. Here, we demonstrate an unprecedented interaction of two phytoalexin classes (Fig. 2) that leads to an increase in the enzymatic formation activity of one of the defense compounds, ultimately resulting in increased levels of scopoletin glucoside and synergistic enhancement of plant resistance. This interplay of the two classes of plant metabolites was accidentally elucidated biochemically by a detailed study of the UDP- α -glucose glucohydrolase activity of NbUGT72AY1 and finally confirmed in tobacco plants. In addition, apocarotenoids are volatile and therefore could affect the function of NbUGT72AY1 at distant sites in the plant. The identification of this novel mechanism should direct the focus of future investigations to similar relationships.

As the carotenoid precursor molecules of apocarotenoids are compartmentalized in plastids, decompartmentalization likely helps plants to recognize tissue damage (Fig. 7). This implies that when plant cells are severely damaged, which includes plastid disruption; apocarotenoids are formed that significantly increase the production of hydroxycoumarin glucosides in neighboring cells. In this scenario, the recently described enzymatic reduction in ionones to ionols by aldo-keto reductases actually enhances the effect of apocarotenoids on the enzymatic activity of NbUGT72AY1 (Koschmieder *et al.*, 2021). Consequently, apocarotenoids serve as specific damage-associated molecular patterns (DAMPs) that amplify the plant resistance mechanisms of hydroxycoumarins (Erb & Kliebenstein, 2020).

Acknowledgements

We thank Johannes Buchner, Chair of Biotechnology for the measurements using analytical centrifugation. We acknowledge Franziska Hackbarth for technical assistance and Miriam Abele for her mass spectrometric support at the BayBioMS. We thank Jonathan Schwab for providing the 3D view of Fig. 6. This research was supported by DFG SCHW 634/34-1. Open Access funding enabled and organized by Projekt DEAL.




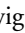
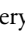



Competing interests

None declared.

Author contributions

GS, JL, EK, TH, WSt and WSc designed experiments and interpreted data. RH and LM planned and performed the plant experiments. EK, TH, TDH, CS, RH, WSt, KM and WSc wrote the manuscript. JL, GS, TJ and EK performed biochemical analyses and analyzed the proteins. JL, GS, EK, TH and CL performed LC-MS/MS analyses. DAMC conducted and evaluated SV-AUC analysis. WSt performed HDX-MS experiments and analyzed HDX-MS data. WSc performed *in silico* analyses. CS, TJ, TDH and WSt contributed to materials, instruments, data analysis, and manuscript. All authors approved the final manuscript. GS and JL contributed equally to this work.

ORCID

Ruth Habegger  <https://orcid.org/0000-0003-2149-9632>
Timothy D. Hoffmann  <https://orcid.org/0000-0001-8505-7126>
Elisabeth Kurze  <https://orcid.org/0000-0001-8625-0737>
Christina Ludwig  <https://orcid.org/0000-0002-6131-7322>
Kate McGraphery  <https://orcid.org/0000-0003-1139-6672>
Wilfried Schwab  <https://orcid.org/0000-0002-9753-3967>
Chuankui Song  <https://orcid.org/0000-0002-7852-1194>
Wieland Steinchen  <https://orcid.org/0000-0003-2990-3660>

Data availability

The proteomics raw data, MAXQUANT search results, and used protein sequence database have been deposited with the ProteomeXchange Consortium via the PRIDE partner repository (<https://www.ebi.ac.uk/pride/>) and can be accessed using the dataset identifier PXD035955 (reviewer account username: reviewer_pxd035955@ebi.ac.uk, password: 4pX4akyO). All other relevant data generated in this study are provided in the main text and the [Supporting Information](#).

References

Baldacci-Cresp F, Le Roy J, Huss B, Lion C, Créach A, Spriet C, Duponchel L, Biot C, Baucher M, Hawkins S *et al.* 2020. UDP-glycosyltransferase 72E3

- plays a role in lignification of secondary cell walls in *Arabidopsis*. *International Journal of Molecular Sciences* 21: 6094.
- Beltran JCM, Stange C. 2016. Apocarotenoids: a new carotenoid-derived pathway. *Sub-Cellular Biochemistry* 79: 239–272.
- Beyer SF, Beesley A, Rohmann PFW, Schultheiss H, Conrath U, Langenbach CJG. 2019. The *Arabidopsis* non-host defence-associated coumarin scopoletin protects soybean from Asian soybean rust. *The Plant Journal* 99: 397–413.
- Bouwmeester H, Schuurink RC, Bleeker PM, Schiestl F. 2019. The role of volatiles in plant communication. *The Plant Journal* 100: 892–907.
- Bowles D, Lim E-K, Poppenberger B, Vaistij FE. 2006. Glycosyltransferases of lipophilic small molecules. *Annual Review of Plant Biology* 57: 567–597.
- Brambilla A, Sommer A, Ghirardo A, Wenig M, Knappe C, Weber B, Amesmaier M, Lenk M, Schnitzler J-P, Vlot AC. 2022. Immunity-associated volatile emissions of β -ionone and nonanal propagate defence responses in neighbouring barley plants. *Journal of Experimental Botany* 73: 615–630.
- Bruder M, Polo G, Trivella DBB. 2020. Natural allosteric modulators and their biological targets: molecular signatures and mechanisms. *Natural Product Reports* 37: 488–514.
- Carter M, Jemth A-S, Carreras-Puigvert J, Herr P, Martínez Carranza M, Vallin KSA, Throup A, Helleday T, Stenmark P. 2018. Human NUDT22 is a UDP-glucose/galactose hydrolase exhibiting a unique structural fold. *Structure* 26: 295–303.
- Chong J, Baltz R, Schmitt C, Beffa R, Fritig B, Saindrenan P. 2002. Downregulation of a pathogen-responsive tobacco UDP-Glc: phenylpropanoid glucosyltransferase reduces scopoletin glucoside accumulation, enhances oxidative stress, and weakens virus resistance. *Plant Cell* 14: 1093–1107.
- Ciesla WP, Bobak DA. 1998. *Clostridium difficile* toxins A and B are cation-dependent UDP-glucose hydrolases with differing catalytic activities. *Journal of Biological Chemistry* 273: 16021–16026.
- Cornish-Bowden A. 2014. Understanding allosteric and cooperative interactions in enzymes. *FEBS Journal* 281: 621–632.
- Dam J, Velikovskiy CA, Mariuzza RA, Urbanek C, Schuck P. 2005. Sedimentation velocity analysis of heterogeneous protein-protein interactions: Lamm equation modeling and sedimentation coefficient distributions $c(s)$. *Biophysical Journal* 89: 619–634.
- Enzell CR. 1985. Biodegradation of carotenoids – an important route to aroma compounds. *Pure and Applied Chemistry* 57: 693–700.
- Erb M, Kliebenstein DJ. 2020. Plant secondary metabolites as defenses, regulators, and primary metabolites: the blurred functional trichotomy. *Plant Physiology* 184: 39–52.
- Fischer A, Smieško M. 2021. A conserved allosteric site on drug-metabolizing CYPs: a systematic computational assessment. *International Journal of Molecular Sciences* 22: 13215.
- Gachon C, Baltz R, Saindrenan P. 2004. Over-expression of a scopoletin glucosyltransferase in *Nicotiana tabacum* leads to precocious lesion formation during the hypersensitive response to tobacco mosaic virus but does not affect virus resistance. *Plant Molecular Biology* 54: 137–146.
- Gai Y-P, Han X-J, Li Y-Q, Yuan C-Z, Mo Y-Y, Guo F-Y, Liu Q-X, Ji X-L. 2014. Metabolomic analysis reveals the potential metabolites and pathogenesis involved in mulberry yellow dwarf disease. *Plant, Cell & Environment* 37: 1474–1490.
- Graña E, Costas-Gil A, Longueira S, Celeiro M, Teijeira M, Reigosa MJ, Sánchez-Moreiras AM. 2017. Auxin-like effects of the natural coumarin scopoletin on *Arabidopsis* cell structure and morphology. *Journal of Plant Physiology* 218: 45–55.
- Grancharov K. 2001. Natural and synthetic inhibitors of UDP-glucuronosyltransferase. *Pharmacology & Therapeutics* 89: 171–186.
- Grant GA. 2018. The many faces of partial inhibition: revealing imposters with graphical analysis. *Archives of Biochemistry and Biophysics* 653: 10–23.
- Gutiérrez-Mellado M-C, Edwards R, Tena M, Cabello F, Serghini K, Jorrín J. 1996. The production of coumarin phytoalexins in different plant organs of sunflower (*Helianthus annuus* L.). *Journal of Plant Physiology* 149: 261–266.
- Hardy JA, Wells JA. 2004. Searching for new allosteric sites in enzymes. *Current Opinion in Structural Biology* 14: 706–715.
- Harrus D, Khoder-Agha F, Peltoniemi M, Hassinen A, Ruddock L, Kellokumpu S, Glumoff T. 2018. The dimeric structure of wild-type human glycosyltransferase B4GalT1. *PLoS ONE* 13: e0205571.
- Hou X, Rivers J, León P, McQuinn RP, Pogson BJ. 2016. Synthesis and function of apocarotenoid signals in plants. *Trends in Plant Science* 21: 792–803.
- Huang F-C, Horváth G, Molnár P, Turcsi E, Deli J, Schrader J, Sandmann G, Schmidt H, Schwab W. 2009. Substrate promiscuity of RdCCD1, a carotenoid cleavage oxygenase from *Rosa damascena*. *Phytochemistry* 70: 457–464.
- van Janse Rensburg HC, van den Ende W. 2017. UDP-Glucose: a potential signaling molecule in plants? *Frontiers in Plant Science* 8: 2230.
- Jeandet P. 2015. Phytoalexins: current progress and future prospects. *Molecules* 20: 2770–2774.
- Jumper J, Evans R, Pritzel A, Green T, Figurnov M, Ronneberger O, Tunyasuvunakool K, Bates R, Židek A, Potapenko A *et al.* 2021. Highly accurate protein structure prediction with ALPHAFOLD. *Nature* 596: 583–589.
- Kai K, Mizutani M, Kawamura N, Yamamoto R, Tamai M, Yamaguchi H, Sakata K, Shimizu B. 2008. Scopoletin is biosynthesized via ortho-hydroxylation of feruloyl CoA by a 2-oxoglutarate-dependent dioxygenase in *Arabidopsis thaliana*. *The Plant Journal* 55: 989–999.
- Kim YH, Choi DI, Yeo WH, Kim YS, Chae SY, Park EK, Kim SS. 2000. Scopoletin production related to induced resistance of tobacco plants against tobacco mosaic virus. *Plant Pathology Journal* 16: 264–268.
- Konermann L, Pan J, Liu Y-H. 2011. Hydrogen exchange mass spectrometry for studying protein structure and dynamics. *Chemical Society Reviews* 40: 1224–1234.
- Koschmieder J, Wüst F, Schaub P, Álvarez D, Trautmann D, Krischke M, Rustenholz C, Mano J, Mueller MJ, Bartels D *et al.* 2021. Plant apocarotenoid metabolism utilizes defense mechanisms against reactive carbonyl species and xenobiotics. *Plant Physiology* 185: 331–351.
- Lanot A, Hodge D, Jackson RG, George GL, Elias L, Lim E-K, Vaistij FE, Bowles DJ. 2006. The glucosyltransferase UGT72E2 is responsible for monolignol 4-O-glucoside production in *Arabidopsis thaliana*. *The Plant Journal* 48: 286–295.
- Le Roy J, Huss B, Creach A, Hawkins S, Neutelings G. 2016. Glycosylation is a major regulator of phenylpropanoid availability and biological activity in plants. *Frontiers in Plant Science* 7: 735.
- Levanova N, Mattheis C, Carson D, To K-N, Jank T, Frankel G, Aktories K, Schroeder GN. 2019. The Legionella effector LtpM is a new type of phosphoinositide-activated glucosyltransferase. *Journal of Biological Chemistry* 294: 2862–2879.
- Liang D-M, Liu J-H, Wu H, Wang B-B, Zhu H-J, Qiao J-J. 2015. Glycosyltransferases: mechanisms and applications in natural product development. *Chemical Society Reviews* 44: 8350–8374.
- Liao J, Sun G, Kurze E, Steinchen W, Hoffmann TD, Song C, Zou Z, Hoffmann T, Schwab WG. 2022. Subfunctionalization of a monolignol to a phytoalexin glucosyltransferase is accompanied by substrate inhibition. *Plant Communications* 4: 100506.
- Luukkanen L, Taskinen J, Kurkela M, Kostiaainen R, Hirvonen J, Finel M. 2005. Kinetic characterization of the 1A subfamily of recombinant human UDP-glucuronosyltransferases. *Drug Metabolism and Disposition* 33: 1017–1026.
- Masson GR, Burke JE, Ahn NG, Anand GS, Borchers C, Brier S, Bou-Assaf GM, Engen JR, Englander SW, Faber J *et al.* 2019. Recommendations for performing, interpreting and reporting hydrogen deuterium exchange mass spectrometry (HDX-MS) experiments. *Nature Methods* 16: 595–602.
- Matros A, Mock H-P. 2004. Ectopic expression of a UDP-glucose: phenylpropanoid glucosyltransferase leads to increased resistance of transgenic tobacco plants against infection with Potato Virus Y. *Plant & Cell Physiology* 45: 1185–1193.
- McGraphery K, Schwab W. 2020. Comparative analysis of high-throughput assays of family-1 plant glycosyltransferases. *International Journal of Molecular Sciences* 21: 6.
- Monod J, Wyman J, Changeux J-P. 1965. On the nature of allosteric transitions: a plausible model. *Journal of Molecular Biology* 12: 88–118.
- Murashige T, Skoog F. 1962. A revised medium for rapid growth and bio assays with tobacco tissue cultures. *Physiologia Plantarum* 15: 473–497.

- Murata M, Kobayashi T, Seo S. 2019. α -Ionone, an apocarotenoid, induces plant resistance to western flower thrips, *Frankliniella occidentalis*, independently of jasmonic acid. *Molecules* 25: 17.
- Nisar N, Li L, Lu S, Khin NC, Pogson BJ. 2015. Carotenoid metabolism in plants. *Molecular Plant* 8: 68–82.
- Offen W, Martinez-Fleites C, Yang M, Kiat-Lim E, Davis BG, Tarling CA, Ford CM, Bowles DJ, Davies GJ. 2006. Structure of a flavonoid glucosyltransferase reveals the basis for plant natural product modification. *EMBO Journal* 25: 1396–1405.
- Paparella A, Shaltiel-Harpaza I, Ibdah M. 2021. β -Ionone: its occurrence and biological function and metabolic engineering. *Plants* 10: 754.
- Peng H, Yang T, Whitaker BD, Shangguan L, Fang J. 2016. Calcium/calmodulin alleviates substrate inhibition in a strawberry UDP-glucosyltransferase involved in fruit anthocyanin biosynthesis. *BMC Plant Biology* 16: 197.
- Rangarajan ES, Proteau A, Cui Q, Logan SM, Potetinova Z, Whitfield D, Purisima EO, Cygler M, Matte A, Sulea T *et al.* 2009. Structural and functional analysis of *Campylobacter jejuni* PseG: a udp-sugar hydrolase from the pseudaminic acid biosynthetic pathway. *Journal of Biological Chemistry* 284: 20989–21000.
- Robe K, Izquierdo E, Vignols F, Rouached H, Dubos C. 2021. The coumarins: secondary metabolites playing a primary role in plant nutrition and health. *Trends in Plant Science* 26: 248–259.
- Romera FJ, García MJ, Lucena C, Martínez-Medina A, Aparicio MA, Ramos J, Alcántara E, Angulo M, Pérez-Vicente R. 2019. Induced systemic resistance (ISR) and Fe deficiency responses in dicot plants. *Frontiers in Plant Science* 10: 287.
- Salt SD, Tuzun S, Kuć J. 1986. Effects of β -ionone and abscisic acid on the growth of tobacco and resistance to blue mold. Mimicry of effects of stem infection by *Peronospora tabacina* Adam. *Physiological and Molecular Plant Pathology* 28: 287–297.
- Schwartz SH, Tan BC, Gage DA, Zeevaert JA, McCarty DR. 1997. Specific oxidative cleavage of carotenoids by VP14 of maize. *Science* 276: 1872–1874.
- Sheikh MO, Halmo SM, Patel S, Middleton D, Takeuchi H, Schafer CM, West CM, Haltiwanger RS, Avci FY, Moremen KW *et al.* 2017. Rapid screening of sugar-nucleotide donor specificities of putative glycosyltransferases. *Glycobiology* 27: 206–212.
- Sindhuwinata N, Grimm LL, Weißbach S, Zinn S, Munoz E, Palcic MM, Peters T. 2013. Thermodynamic signature of substrates and substrate analogs binding to human blood group B galactosyltransferase from isothermal titration calorimetry experiments. *Biopolymers* 99: 784–795.
- Speckaert N, Adamou NM, Hassane HA, Baldacci-Cresp F, Mol A, Goeminne G, Boerjan W, Duez P, Hawkins S, Neutelings G *et al.* 2020. Characterization of the UDP-glycosyltransferase UGT72 family in poplar and identification of genes involved in the glycosylation of monolignols. *International Journal of Molecular Sciences* 21: 5018.
- Speckaert N, El Jaziri M, Baucher M, Behr M. 2022. UGT72, a major glycosyltransferase family for flavonoid and monolignol homeostasis in plants. *Biology* 11: 441.
- Stringlis IA, De JR, Pieterse CMJ. 2019. The age of coumarins in plant–microbe interactions. *Plant & Cell Physiology* 60: 1405–1419.
- Sun G, Putkaradze N, Bohnacker S, Jonczyk R, Fida T, Hoffmann T, Bernhardt R, Härtl K, Schwab W. 2020. Six uridine-diphosphate glycosyltransferases catalyze the glycosylation of bioactive C₁₃-apocarotenols. *Plant Physiology* 184: 1744–1761.
- Sun G, Strebl M, Merz M, Blamberg R, Huang F-C, McGraphery K, Hoffmann T, Schwab W. 2019. Glucosylation of the phytoalexin N-feruloyl tyramine modulates the levels of pathogen-responsive metabolites in *Nicotiana benthamiana*. *The Plant Journal* 100: 20–37.
- Sun H, Song N, Ma L, Li J, Wu J. 2017. Ethylene signalling is essential for the resistance of *Nicotiana attenuata* against *Alternaria alternata* and phytoalexin scopoletin biosynthesis. *Plant Pathology* 66: 277–284.
- Sun H, Wang L, Zhang B, Ma J, Hettenhausen C, Cao G, Sun G, Wu J. 2014. Scopoletin is a phytoalexin against *Alternaria alternata* in wild tobacco dependent on jasmonate signalling. *Journal of Experimental Botany* 65: 4305–4315.
- Sun T, Yuan H, Cao H, Yazdani M, Tadmor Y, Li L. 2018. Carotenoid metabolism in plants: the role of plastids. *Molecular Plant* 11: 58–74.
- Torres-Montilla S, Rodriguez-Concepcion M. 2021. Making extra room for carotenoids in plant cells: new opportunities for biofortification. *Progress in Lipid Research* 84: 101128.
- Uchaipichat V, Galetin A, Houston JB, Mackenzie PI, Williams JA, Miners JO. 2008. Kinetic modeling of the interactions between 4-methylumbelliferone, 1-naphthol, and zidovudine glucuronidation by UDP-glucuronosyltransferase 2B7 (UGT2B7) provides evidence for multiple substrate binding and effector sites. *Molecular Pharmacology* 74: 1152–1162.
- Wahlberg I, Enzell CR. 1987. Tobacco isoprenoids. *Natural Product Reports* 4: 237–276.
- Wang Y, Chantreau M, Sibout R, Hawkins S. 2013. Plant cell wall lignification and monolignol metabolism. *Frontiers in Plant Science* 4: 220.
- Wyatt SE. 1992. The accumulation of β -ionone and 3-hydroxy esters of β -ionone in tobacco immunized by foliar inoculation with tobacco mosaic virus. *Phytopathology* 82: 580.
- Yonekura-Sakakibara K, Hanada K. 2011. An evolutionary view of functional diversity in family 1 glycosyltransferases. *The Plant Journal* 66: 182–193.
- Zhang H, Zhu F, Yang T, Ding L, Zhou M, Li J, Haslam SM, Della A, Erlandsen H, Wu H. 2014. The highly conserved domain of unknown function 1792 has a distinct glycosyltransferase fold. *Nature Communications* 5: 4339.
- Zhang J, Banks DD, He F, Treuheit MJ, Becker GW. 2015. Effects of sucrose and benzyl alcohol on GCSF conformational dynamics revealed by hydrogen deuterium exchange mass spectrometry. *Journal of Pharmaceutical Sciences* 104: 1592–1600.
- Zhang M, Yi Y, Gao B-H, Su H-F, Bao Y-O, Shi X-M, Wang H-D, Li F-D, Ye M, Qiao X. 2022. Functional characterization and protein engineering of a triterpene 3-/6-/12'-O-glycosyltransferase reveal a conserved residue critical for the regioselectivity. *Angewandte Chemie (International ed. in English)* 61: e202113587.
- Zorn JA, Wells JA. 2010. Turning enzymes ON with small molecules. *Nature Chemical Biology* 6: 179–188.

Supporting Information

Additional Supporting Information may be found online in the Supporting Information section at the end of the article.

Dataset S1 Overview of data obtained by hydrogen/deuterium exchange mass spectrometry.

Fig. S1 Products formed by NbUGT72AY1.

Fig. S2 Products formed by NbUGT72AY1.

Fig. S3 Products formed by NbUGT72AY1.

Fig. S4 UDP-glucose glucohydrolase activity of NbUGT72AY as a function of UDP-glucose concentration and inhibition by ionols.

Fig. S5 UDP-glucose glucohydrolase activity of NbUGT72AY is inhibited by ionols.

Fig. S6 Inhibition of UDP-glucose glucohydrolase activity of NbUGT72AY1 by ionols and ionones as a function of ionol/ionone concentration.

Fig. S7 Effect of co-incubation of apocarotenoids on the glucose levels was analyzed by liquid chromatography-mass spectrometry.

Fig. S8 Activation of the UDP-glucose:scopoletin glucosyltransferase activity of NbUGT72AY1 by ionols, ionones, and damascones.

Fig. S9 Activation of the UDP-glucose:umbelliferone glucosyltransferase activity of NbUGT72AY1 by ionols, ionones, and damascones.

Fig. S10 UDP-glucose:conferyl aldehyde glucosyltransferase activity of NbUGT72AY1 is unaffected by ionols, ionones, and damascones.

Fig. S11 Determination of oligomeric states of NbUGT72AY1 based on Native-PAGE gel and analytical ultracentrifugation.

Fig. S12 Liquid chromatography-mass spectrometry/mass spectrometry analysis of NbUGT72AY1 bands from SDS-PAGE and Native-PAGE gels.

Fig. S13 UDP-glucose glucohydrolase activity of His-tagged and GST-tagged NbUGT72AY1.

Fig. S14 HDX-MS of apo NbUGT72AY1.

Fig. S15 Conformational changes in NbUGT72AY1 related to binding of scopoletin.

Fig. S16 Conformational changes in NbUGT72AY1 related to α -ionol-binding.

Fig. S17 Conformational changes in NbUGT72AY1 related to α -ionone-binding.

Fig. S18 Conformational changes in NbUGT72AY1 related to β -ionol-binding.

Fig. S19 Conformational changes in NbUGT72AY1 related to β -ionone-binding.

Fig. S20 Conformational changes in NbUGT72AY1 related to substrate binding.

Fig. S21 Conformational changes in NbUGT72AY1 related to substrate binding.

Fig. S22 Reduction in substrate inhibition of NbUGT72AY1 by apocarotenoids as determined by liquid chromatography-mass spectrometry analysis.

Fig. S23 Ionol glucosyltransferase activity of NbUGT72AY1 determined by liquid chromatography-mass spectrometry analysis.

Please note: Wiley is not responsible for the content or functionality of any Supporting Information supplied by the authors. Any queries (other than missing material) should be directed to the *New Phytologist* Central Office.